

# 1 Comparison of SMOS and SMAP soil moisture retrieval approaches using 2 tower-based radiometer data over a vineyard field

3  
4 Maciej Miernecki<sup>a</sup>, Jean-Pierre Wigneron<sup>b</sup>, Ernesto Lopez-Baeza<sup>c</sup>, Yann Kerr<sup>d</sup>, Richard De Jeu<sup>c</sup>,  
5 Gabrielle J. M. De Lannoy<sup>f</sup>, Tom J. Jackson<sup>g</sup>, Peggy E. O'Neill<sup>f</sup>, Mike Schwank<sup>h,i</sup>, Roberto Fernandez  
6 Moran<sup>c</sup>, Simone Bircher<sup>d</sup>, Heather Laurence<sup>j</sup>, Arnaud Mialon<sup>d</sup>, Ahmad Al Bitar<sup>d</sup>, Philippe Richaume<sup>d</sup>  
7

8 <sup>a</sup> University of Hamburg, Center for Marine and Atmospheric Sciences (ZMAW), Hamburg, Germany

9 <sup>b</sup> INRA, Bordeaux Sciences Agro, UMR 1391 ISPA, F-33140 Villenave d'Ornon, France

10 <sup>c</sup> Faculty of Physics, University of Valencia, 50. Burjassot. 46100 Valencia, Spain

11 <sup>d</sup> Centre d'Etudes Spatiales de la Biosphère (CESBIO — CNES, CNRS, IRD, Université Toulouse  
12 III), Toulouse, France

13 <sup>e</sup> Department of Earth Sciences, VU University Amsterdam, the Netherlands.

14 <sup>f</sup> NASA GSFC, Greenbelt, MD 20771, USA

15 <sup>g</sup> USDA-ARS Hydrology and Remote Sensing Laboratory, Beltsville, MD 20705-2350 USA

16 <sup>h</sup> Gamma Remote Sensing, Worbstr. 225, CH-3073 Gümliigen, Switzerland

17 <sup>i</sup> Swiss Federal Research Institute WSL, Zürcherstrasse 111, 8903 Birmensdorf, Switzerland

18 <sup>j</sup> European Centre for Medium-Range Weather Forecasts (ECMWF), Reading, UK

## 19 20 21 **ABSTRACT**

22 The objective of this study was to compare several approaches to soil moisture (SM) retrieval  
23 using L-band microwave radiometry. The comparison was based on a brightness temperature  
24 ( $T_B$ ) data set acquired since 2010 by the L-band radiometer ELBARA-II over a vineyard field  
25 at the Valencia Anchor Station (VAS) site. ELBARA-II, provided by the European Space  
26 Agency (ESA) within the scientific program of the SMOS (Soil Moisture and Ocean Salinity)  
27 mission, measures multiangular  $T_B$  data at horizontal and vertical polarization for a range of  
28 incidence angles (30°-60°). Based on a three year data set (2010-2012), several SM retrieval  
29 approaches developed for spaceborne missions including AMSR-E (Advanced Microwave  
30 Scanning Radiometer for EOS), SMAP (Soil Moisture Active Passive) and SMOS were  
31 compared. The approaches include: the Single Channel Algorithm (SCA) for horizontal  
32 (SCA-H) and vertical (SCA-V) polarizations, the Dual Channel Algorithm (DCA), the Land

33 Parameter Retrieval Model (LPRM) and two simplified approaches based on statistical  
34 regressions (referred to as 'Mattar' and 'Saleh'). Time series of vegetation indices required for  
35 three of the algorithms (SCA-H, SCA-V and 'Mattar') were obtained from MODIS  
36 observations. The SM retrievals were evaluated against reference SM values estimated from a  
37 multiangular 2-Parameter inversion approach. The results obtained with the current base line  
38 algorithms developed for SMAP (SCA-H and -V) are in very good agreement with the  
39 'reference' SM data set derived from the multi-angular observations ( $R^2 \approx 0.90$ ,  
40 RMSE varying between 0.035 and 0.056  $m^3/m^3$  for several retrieval configurations). This  
41 result showed that, provided the relationship between vegetation optical depth and a remotely-  
42 sensed vegetation index can be calibrated, the SCA algorithms can provide results very close  
43 to those obtained from multi-angular observations in this study area. The approaches based on  
44 statistical regressions provided similar results and the best accuracy was obtained with the  
45 'Saleh' methods based on either bi-angular or bipolarization observations ( $R^2 \approx 0.93$ ,  
46 RMSE  $\approx 0.035 m^3/m^3$ ). The LPRM and DCA algorithms were found to be slightly less  
47 successful in retrieving the 'reference' SM time series ( $R^2 \approx 0.75$ , RMSE  $\approx 0.055 m^3/m^3$ ).  
48 However, the two above approaches have the great advantage of not requiring any model  
49 calibrations previous to the SM retrievals.

50

## 51 **1. Introduction**

52 Surface soil moisture plays a major role in the water and energy budgets of continental  
53 surfaces, which has direct implications for hydrological, climate, and weather forecasting  
54 models. L-band passive microwave remote sensing is one of the most promising approaches  
55 to monitor this variable at the global scale with frequent revisiting times (Jackson et al., 1995;  
56 Kerr et al., 2001, Njoku et al., 2003; De Lannoy et al., 2013). Three recent or planned space  
57 missions use this technology: SMOS (launched end of 2009), Aquarius (launched in June of  
58 2011) and SMAP (launch scheduled in November 2014).

59 The Soil Moisture and Ocean Salinity (SMOS) mission is the first spaceborne mission  
60 dedicated to soil moisture (SM) mapping. SMOS has multi-angular capabilities which are  
61 exploited by the SM retrieval approach: SM and vegetation optical depth  $\tau$  (used to  
62 parameterize vegetation attenuation and emission) are retrieved simultaneously based on  
63 SMOS multi-configuration observations, in terms of polarizations and incidence angles.  
64 Aquarius is a combined passive/active L-band microwave instrument which consists of a set

65 of three radiometers and a scatterometer, operating at 1.4 GHz and 1.26 GHz respectively  
66 (Levine et al., 2010). The primary mission objective of Aquarius is to provide global  
67 observations of surface sea salinity once every 7 days. However, Aquarius has also potential  
68 capabilities to monitor soil moisture at global scales (Luo et al., 2013, Bindlish et al., 2013).  
69 SMAP incorporates a radar and a radiometer, both operating at L-band and at the incidence  
70 (observation) angle  $\theta = 40^\circ$ . The spatial resolutions of the corresponding active- and passive  
71 microwave signatures are  $\sim 39 \text{ km} \times 47 \text{ km}$  and  $\sim 1 \text{ km} \times 1 \text{ km}$ , respectively. The mission  
72 concept is to combine the complementary attributes of the radar observations (high spatial  
73 resolution but lower soil moisture accuracy) and radiometer observations (higher soil moisture  
74 accuracy but coarse spatial resolution) to retrieve SM at a spatial resolution of 9 km, and the  
75 freeze-thaw state at a spatial resolution of 3 km (Entekhabi et al., 2010; O'Neill et al., 2013).  
76 Several SM retrieval approaches have been developed in the context of these L-band space  
77 missions. As noted above, in the operational SMOS SM retrieval algorithm, SM and  
78 vegetation optical depth at nadir ( $\tau_{\text{NAD}}$ ) are retrieved simultaneously based on SMOS  
79 multiangular and bipolarization observations (Wigneron et al., 1995, 2000; Kerr et al., 2012).  
80 The 2-Parameter (2-P) retrievals of SM and  $\tau_{\text{NAD}}$  are obtained from inversion of the L-MEB  
81 (L-band Microwave Emission of the Biosphere) model (Wigneron et al., 2007). This forward  
82 model is based on the so-called  $\tau$ - $\omega$  model (Mo et al., 1982) and it includes a number of  
83 parameterizations to capture effects of vegetation structure and soil roughness on polarization  
84 and angular properties of L-band  $T_{\text{B}}$  emitted from land surfaces. The inversion of L-MEB  
85 considering SM and  $\tau_{\text{NAD}}$  as the requested parameters (referred to as 'L-MEB 2-P' inversion)  
86 is implemented in the operational algorithms used to compute the Level 2 (distributed by  
87 ESA) and Level 3 (distributed by the Centre Aval de Traitement des Données SMOS  
88 (CATDS), Berthon et al., 2012) SMOS products. In parallel to this operational retrieval  
89 method, several simplified methods have been developed to exploit the capability of L-band  
90 radiometers to provide information on land surface states such as SM. For instance, Wigneron  
91 et al. (2004) and Saleh et al. (2006) have evaluated statistical regressions based on bi-  
92 polarization or bi-angular  $T_{\text{B}}$  data. Mattar et al. (2012) have evaluated similar regression  
93 methods that also use a vegetation index estimated from ancillary remotely sensed  
94 observations (such as the Normalized Difference Vegetation Index (NDVI) or the Leaf Area  
95 Index (LAI)) to account for vegetation effects. Moreover, methods based on Neural Networks  
96 have been and are currently evaluated (Liu et al., 2002; Rodriguez et al., 2003).

97 The general retrieval approach proposed for SMAP is different from the operational SMOS  
98 SM retrieval: SMAP observations will be available for the sole incidence angle of  $40^\circ$ , but  
99 make use of the complementary information provided by the active- (radar) and the passive  
100 (radiometer) L-band data. In the initial release of the ATBD (Algorithm Theoretical Basis  
101 Document) written for the retrievals from SMAP's radiometer (O'Neill et al., 2013), four soil  
102 moisture retrieval algorithms are suggested for evaluation during the pre- and post-launch  
103 calibration and validation activities: (i) the single-channel algorithm at H polarization (SCA-  
104 H) which is the current SMAP baseline algorithm, (ii) the single-channel algorithm at V  
105 polarization (SCA-V), (iii) the dual-channel algorithm (DCA), and (iv) the Land parameter  
106 retrieval model (LPRM). In the SCA-H and -V algorithms, vegetation is accounted for by the  
107  $\tau$ - $\omega$  model as in L-MEB. However, optical depth at nadir ( $\tau_{\text{NAD}}$ ) is not retrieved as for SMOS.  
108 Instead it is estimated from the linear relation  $\tau_{\text{NAD}} = b \cdot \text{VWC}$  between  $\tau_{\text{NAD}}$  and vegetation  
109 water content (VWC) (Jackson et al. (1991)). Thereby, values of the b-parameter are assumed  
110 polarization independent and will be provided from a land cover look up table, and the VWC  
111 is estimated from values of the NDVI Index. The DCA retrieval approach is very similar to  
112 the one used for SMOS. The only difference is that the inversion is based on the minimization  
113 of a cost function accounting for the Root Mean Square Error (RMSE) between measured and  
114 simulated bi-polarized  $T_B$  observations at one incidence angle, whereas multi-angular  
115 observations are used for SMOS. In the LPRM algorithm, the Microwave Polarization  
116 Difference Index (MPDI) and the observed emissivities are used to derive the vegetation  
117 optical depth  $\tau$  (Meesters et al., 2005). In a second step, SM is retrieved with an optimization  
118 routine that minimizes the error between the modelled and observed H-polarized brightness  
119 temperatures (Owe et al., 2008; De Jeu et al., 2009).

120 In this study, these different retrieval algorithms were compared using a 3-year long  
121 multiangular  $T_B$  data set acquired by the L-band radiometer ELBARA-II over a vineyard field  
122 (MELBEX-III) at the Valencia Anchor Station (VAS) site (Schwank et al., 2012, Wigneron et  
123 al., 2012). Applications of the retrieval methods can be made at large scales from satellite  
124 observations but also at more local scale for long term SM monitoring from ground based  
125 instruments mounted on different types of platforms: towers as for ELBARA-II (de Rosnay et  
126 al., 2006; Schwank et al., 2012; Schlenz et al., 2012, etc.); trucks (Hornbuckle et al., 2004;  
127 Kurum et al., 2009) or from the top of a mountain as in Pellarin et al. (2013).

128 ELBARA-II (Schwank et al. 2010), developed by GAMMA Remote Sensing AG  
129 (Switzerland) and funded by the ESA, provides  $T_B$  at horizontal and vertical polarization for a

130 range of observation angles ( $30^{\circ}$ - $60^{\circ}$ ). The ELBARA-II  $T_B$  observations were acquired since  
131 2010 and a 3-year  $T_B$  data set is available for the MELBEX-III site. As an accurate estimation  
132 of SM from ground based measurements over the MELBEX-III site could not be achieved  
133 because of very frequent agricultural practices within the field, it was considered that  
134 representative SM values (referred to as 'reference' SM data set) over the ELBARA-II  
135 footprints were obtained from multi-angular 2-P L-MEB retrievals. Moreover, the 2-P L-MEB  
136 approach also provided retrievals of optical depth at nadir ( $\tau_{NAD}$ ). These latter values were  
137 used to calibrate the relationships between  $\tau_{NAD}$  and NDVI, which are required in the SCA-H  
138 and SCA-V algorithms. Based on these 'reference' SM and  $\tau_{NAD}$  data sets and the ELBARA-  
139 II  $T_B$  observations, seven SM retrieval approaches were evaluated and compared: the four  
140 methods considered presently in the SMAP ATBD based on bi-polarization observations at  
141 one observation angle ( $\theta = 40^{\circ}$  for SMAP) and three regression methods (Saleh et al, 2006  
142 and Mattar et al., 2012) developed in the framework of SMOS research activities and based  
143 on bi-angular or bipolarization observations. The results of this evaluation are discussed in the  
144 context of the improvement and development of the SM retrieval algorithms.

145

146

## 147 **2. Materials and method**

### 148 **2.1. The ELBARA-II radiometer at MELBEX-III (VAS site)**

149 The study was based on  $T_B$  measurements made by the ELBARA-II radiometer over the  
150 2010-2012 period within the VAS site. ELBARA-II was installed in September 2009 at the  
151 MELBEX-III vineyard field (referred to as M-III), close to Caudete de las Fuentes, on the  
152 Utiel-Requena Plateau at  $\sim 800$  m a.s.l., in the region of Valencia, Spain ( $39^{\circ}31'18.18''N$ ,  
153  $1^{\circ}17'29.64''W$ ). This site is one of the reference sites selected by ESA in Europe within the  
154 SMOS science program.

155 All details concerning the ELBARA-II instrument and the M-III experiment set up are given  
156 in Schwank et al. (2010, 2012), and Wigneron et al. (2012). Only a brief summary of the main  
157 information concerning this experiment is presented here.

158 The ELBARA-II radiometer was set up 17 meters above ground to monitor a vineyard that is  
159 representative of the main land use of the VAS region. The ELBARA-II was equipped with  
160 an elevation tracker that allows measurements at specific observation angles  $\theta$  varying

161 between  $30^\circ \leq \theta \leq 330^\circ$  with  $\theta = 180^\circ$  being the zenith direction. Every 30 minutes,  
162 automated "elevation scans" are carried out that provide  $T_B$  at horizontal and vertical  
163 polarizations at observation angles between  $\theta = 30^\circ$  and  $70^\circ$  with steps of  $5^\circ$ . Between each  
164 elevation scan, measurements are made at the  $\theta = 45^\circ$  every 10 minutes. Once a day, at 23:55  
165 local time, the radiometer is automatically positioned at  $150^\circ$  to carry out sky calibration  
166 measurements. The absolute accuracy of the ELBARA-II measurements was estimated to be  
167 better than  $\pm 1$  K over the course of 2010-2012. During short time periods, no measurement  
168 could be acquired over the vineyard field due to experiments using reflecting foils (Schwank  
169 et al., 2012) or due to technical issues: in 2010 (DoY 222 - DoY 245, DoY 312 - DoY 337)  
170 and in 2011 (DoY 41 - DoY 62; DoY 84 - DoY 133). The ELBARA-II observations were  
171 slightly affected by Radio Frequency Interferences (RFI) caused by active microwave systems  
172 violating the protected part of the L-Band (1400 MHz - 1427 MHz). Efforts made by the  
173 Spanish administrative authorities in 2010 to mitigate RFI disturbances resulted in a  
174 significant decrease since the beginning of July in 2010 (~ DoY 190). Most RFI events result  
175 in steep increases in the time variations of the measured  $T_B$  (larger than 30K at minimum) and  
176 unrealistic  $T_B$  values (larger than 330 K). These RFI events were detected manually from the  
177 ELBARA-II  $T_B$  data set. To be consistent with the overpass times of SMOS and SMAP, only  
178  $T_B$  measurements made at 6 am and 6 pm local time are considered in this study.

179

## 180 **2.2. *In situ* measurements**

181 Concurrent with the ELBARA-II observations, ground measurements were obtained within  
182 the M-III vineyard. Soil profiles of the volumetric soil moisture [ $\text{m}^3 \cdot \text{m}^{-3}$ ] and temperature  
183 were acquired up to about 1 m (Wigneron et al., 2012). Vineyard cultivation practices are  
184 carried out frequently within the field (for weeding and pest control, winter and summer  
185 pruning, cluster thinning, etc.) so that SM probes could not be installed permanently within  
186 the ELBARA-II footprints. Only two Delta-T Theta Probes measuring the volumetric SM of  
187 the top 0-6cm soil layer were installed at the border of the field where no field work was  
188 carried out. It is our opinion that these SM probes cannot provide SM values representative of  
189 the field conditions as seen by the ELBARA-II instrument and have not been used in the  
190 analysis presented here (Wigneron et al., 2012).



191 A meteorological station located at the VAS (coordinates: 39°34'15''N, 1°17'18''W, 813 m  
192 a.s.l.), a few kilometres from the M-III site provided the standard meteorological variables (air  
193 temperature, wind speed, air humidity, etc.). Over the VAS site, the average value of the total  
194 yearly precipitation over the ten years prior to 2010 is  $P = 461$  mm. For the three years  
195 considered in this study; 2010 was wet ( $P = 538.2$  mm) and was followed by a 'dry' and a  
196 'very dry' year in 2011 and 2012 ( $P = 379.2$  mm in 2011 and  $P = 288.6$  mm in 2012).

197 Details concerning the soil and vegetation conditions at the M-III site are provided in  
198 Wigneron et al. (2012). The field-site observed with ELBARA-II is typical of vineyards in the  
199 VAS region (the spacing between each plant is  $\sim 2$  m and that between each row is  $\sim 3$  m).  
200 Two field experiments in 2007 and 2010 led to similar values of the maximum Leaf Area  
201 Index,  $LAI_{MAX} \approx 2.2$ . To monitor the time variations in the vegetation characteristics over the  
202 growing season, we used the NDVI index from the MODIS products (16 day NDVI  
203 composite of 250 m MODIS data; MODIS (2010)). As the field was large enough (larger than  
204 300 m x 300 m), it can be considered that the MODIS NDVI time variations are representative of  
205 the vegetation conditions as seen by the ELBARA-II radiometer operated at the M-III site.

206 In order to monitor the evolution of the surface roughness over time, field measurements were  
207 made by means of measuring mechanically two-dimensional profiles of the ground surface.  
208 For this purpose, a 2 m needle board with 201 needles, movable in the vertical direction and  
209 with 1 cm spacing between needles was used (Mialon et al. (2012)). The needle board was  
210 leveled and placed on the ground such that the needles were allowed to fall until they touched  
211 the soil surface. Subsequently, photos of the profile created by the needle heights were taken  
212 and digitized to compute soil roughness parameters. On each of the seven days during 2012  
213 when roughness measurements were performed, approximately 8 to 12 profiles were taken  
214 within the ELBARA-II footprints. Different locations and orientations (perpendicular and  
215 parallel to the vegetation rows) were considered in computing representative information on  
216 the standard deviation of soil surface height ( $S_D$ , cm), and correlation length ( $L_C$ , cm). Time  
217 variations in the average values of  $S_D$  and  $L_C$  are shown in Fig. 1 for the seven days of  
218 measurements in 2012. The corresponding annual mean values are  $\langle S_D \rangle = 2.2$  cm,  $\langle L_C \rangle$   
219  $= 6.2$  cm.

220

### 221 **2.3 L-MEB modelling and inversion**

222 The data set considered as a reference in this study was obtained using the 2-P L-MEB  
223 inversion approach to obtain retrievals of SM and  $\tau_{\text{NAD}}$  (Wigneron et al., 2000). There are  
224 many reasons to use this retrieved data set as a reference.

225 First, the SM data set retrieved from tower-based remote sensing observations can be  
226 considered as representative of the SM conditions over the whole ELBARA-II footprint (this  
227 is usually a complex task using field probes distributed within the field). Second, the 2-P L-  
228 MEB method, based on multi-angular observations, has been validated in many studies  
229 against experimental data sets for a variety of soil and vegetation conditions (Wigneron et al.,  
230 1995, 2007; Pardé et al., 2003, 2004, Saleh et al., 2006; Panciera et al., 2009; Cano et al.,  
231 2010; Schlenz et al., 2012, etc.), and its accuracy and robustness has been evaluated  
232 theoretically (Wigneron et al., 2000). The 2-P L-MEB method is currently implemented in the  
233 official SMOS retrieval algorithm (Kerr et al, 2012). Third, the 2-P L-MEB approach has the  
234 advantage of providing retrievals of optical depth at nadir ( $\tau_{\text{NAD}}$ ). These latter values were  
235 used to calibrate the relationships between  $\tau_{\text{NAD}}$  and NDVI, which are required in the SCA-H  
236 and SCA-V algorithms. Moreover, it can not be considered that one method can benefit from  
237 the use of 2-P L-MEB retrieval method as a reference: the equations of the L-MEB model,  
238 used in the 2-P L-MEB approach, are also the basis of the SCA-H, SCA-V, DCA and LPRM  
239 algorithms.

240 A detailed description of the L-MEB model is given in Wigneron et al. (2007) and a brief  
241 summary of the main L-MEB equations and of additional parameterizations developed since  
242 2007 is given in the following. The L-MEB model is based on a zero-order solution of the  
243 radiative transfer equations: the so called  $\tau$ - $\omega$  model, where the optical depth  $\tau$  accounts for  
244 extinction effects within the canopy and the effective scattering albedo  $\omega$  (-) accounts for  
245 scattering effects (Mo et al., 1982; Kurum et al., 2013). To incorporate the SMOS multi-  
246 angular feasibility, several additional parameterizations are used in L-MEB to account for  
247 effects of the vegetation structure and soil roughness on L-band brightness temperatures  
248 emitted from vegetated land surfaces.

249 In local thermal equilibrium the emissivity  $e_{\text{GP}}$  of the ground at horizontal ( $p = \text{H}$ ) and vertical  
250 ( $p = \text{V}$ ) polarization is related to the corresponding reflectivity  $r_{\text{GP}}$  of the soil (the ground)  
251 observed at the angle  $\theta$ :

$$252 \quad e_{\text{GP}}(\theta) = 1 - r_{\text{GP}}(\theta) \quad (1)$$



253 The soil reflectivity  $r_{GP}$  can be expressed as the reflectivity  $r_{GP}^*$  of a specular surface and the  
254 roughness model parameters  $Q_R$ ,  $H_R$  and  $N_{RP}$  as:

$$255 \quad r_{GP}(\theta) = [(1-Q_R) r_{GP}^*(\theta) + Q_R r_{GQ}^*(\theta)] \exp(-H_R \cos^{N_{RP}}(\theta)) \quad (2)$$

256 In this equation,  $H_R$  parameterizes the intensity of the roughness effects,  $Q_R$  parameterizes the  
257 polarization mixing effects, and  $N_{RP}$  is used to account for the specific effects of roughness on  
258 the trend of soil reflectivity  $r_{GP}$  as a function of incidence angle and polarization. The  
259 reflectivity of a specular surface  $r_{GP}^*$  was computed using the Fresnel equations as a function  
260 of  $\theta$  and of the effective soil dielectric permittivity  $\epsilon_G$ . The latter was computed from soil  
261 moisture SM, soil effective temperature  $T_G$ , and from the clay fraction using the dielectric  
262 mixing model of Mironov et al. (2012), referred to as the ‘Mironov’ model in the following.  
263 This is in contrast to the earlier study Wigneron et al. (2007), where the Dobson model  
264 (Dobson et al., 1985) was used to estimate  $\epsilon_G$ .

265 We used the recent results of Lawrence et al. (2013) to estimate the values of the roughness  
266 model parameters ( $Q_R$ ,  $H_R$  and  $N_{RP}$ ). These parameters were assumed as constants in time,  
267 and therefore computed from the annual average value  $\langle S_D \rangle$  of the standard deviation of the  
268 soil surface height and the corresponding annual mean  $\langle L_C \rangle$  of the correlation length (Fig. 1).  
269 To be consistent with the general approach considered for SMAP we assumed that  $N_{RV} = N_{RH}$   
270 = 0 (O’Neill et al., 2013). On that assumption, the roughness parameters  $H_R$  and  $Q_R$  were  
271 computed as (Lawrence et al., 2013):

$$272 \quad H_R = 1.762 (1 - \exp(-Z_S/1.85)) \text{ and } Q_R = 0.05 H_R \quad (3)$$

273 where  $Z_S = (S_D)^2 / L_C$  (cm)

274 Considering the annual mean values  $\langle S_D \rangle = 2.2$  cm and  $\langle L_C \rangle = 6.2$  cm measured over the M-III  
275 site in 2012, we obtained  $Z_S = 0.78$  cm,  $H_R = 0.606$ ,  $Q_R = 0.0303$ .

276 In this study, we considered a composite soil-vegetation surface temperature  $T_{GC}$  for the  
277 effective temperature  $T_G$  of the ground (the soil) and the vegetation canopy  $T_C$ . The composite  
278 effective temperature  $T_{GC}$  of the ELBARA-II footprints was computed from the ERA-  
279 INTERIM 0-7 cm soil temperature product ( $T_{E-07}$ ). ERA-INTERIM is the latest ECMWF  
280 (European Centre for Medium-Range Weather Forecasts) global atmospheric reanalysis of the  
281 period 1979 to the present (Dee et al., 2011) with a temporal resolution of 3 hours and a

282 spatial resolution of  $0.75^\circ$  (corresponding to about 100 km resolution over the VAS site). The  
 283 accuracy of this estimate was considered to be sufficient in several studies investigating SM  
 284 retrievals from L-band observations (Pardé et al., 2004; Wigneron et al., 2012).

285 As noted above, we used the  $\tau - \omega$  model to compute the upwelling emission ( $T_B$ ) from the  
 286 two layer soil-vegetation medium.  $T_{BP}$  ( $p = H, V$ ) is the sum of three terms: (1) the direct  
 287 upwelling vegetation emission, (2) the downwelling vegetation emission reflected by the soil  
 288 and attenuated by the canopy layer, and (3) upwelling soil emission attenuated by the canopy:

$$289 \quad T_{BP} = (1-\omega_P) (1-\gamma_P) (1 + \gamma_P r_{GP}) T_C + (1-r_{GP}) \gamma_P T_G \quad (4)$$

290 where  $T_G = T_C = T_{GC} = T_{E-07}$  is assumed in this study, and  $r_{GP}$  is the soil reflectivity computed  
 291 with (2) and (3).  $\gamma_P$  is the vegetation attenuation factor which is related to the optical depth  $\tau_P$   
 292 as (Beer's law):

$$293 \quad \gamma_P = \exp(-\tau_P / \cos \theta) \quad (5)$$

294 To account for vegetation anisotropies, the optical depth  $\tau_P(\theta)$  at the observation angle  $\theta$  is  
 295 expressed with a parameterization involving the optical depth  $\tau_{NAD}$  at nadir ( $\theta = 0^\circ$ ):

$$296 \quad \tau_P(\theta) = \tau_{NAD} (\sin^2(\theta).tt_P + \cos^2(\theta)) \quad (\text{at } p = V, H) \quad (6)$$

297 The parameters  $tt_V$  (-) and  $tt_H$  (-) account for the angular dependence of  $\tau_P(\theta)$ . As found in  
 298 Wigneron et al. (2012), we considered that  $tt_H = 1$  (default L-MEB value) and that the  $tt_V$   
 299 parameter is free in the retrieval process, to account for the effects of the vine stocks, with a  
 300 preferential vertical orientation. So in reality, a 3-Parameter retrieval approach is made in this  
 301 study, but the notation 2-P is kept, as only SM and  $\tau$  can be considered as variables of interest  
 302 for applications.

303 The values of the effective scattering albedo  $\omega_P$  were found to be close to zero over most of  
 304 the non-forested vegetation covers (Grant et al., 2008; Kurum et al., 2013). The value of  $\omega_P$   
 305 was set equal here to 0.02 for both polarizations. A summary of the values of the soil and  
 306 vegetation L-MEB parameters used in this study over the M-III site and described above is  
 307 given in Table 1.

308 The 2-P L-MEB inversions were based on bi-polarization and multiangular  $T_B$  measurements  
 309 using a minimization procedure of a cost function evaluating the difference between the L-

310 MEB simulations and the  $T_B$  measurements (Wigneron et al., 2000, 2007, 2012). The  
311 retrievals were based on ELBARA-II  $T_B$  data acquired with the automated elevation scans  
312 (section 2.1) performed for the observation angles  $\theta = 30^\circ, 35^\circ, 40^\circ, 45^\circ, 50^\circ$  (corresponding  
313 roughly to the limit of validity of L-MEB at large incidence angles). As noted above, only  $T_B$   
314 measurements made at 6 am and 6 pm will be considered in this study. Especially for the  
315 measurements at 6 am temperature gradients across the vegetation and the soil are minimal  
316 (Kerr et al., 2001).

317

## 318 **2.4 Description of the different SM retrieval methods**

319 As mentioned in the introduction, seven SM retrieval approaches were evaluated and  
320 compared in this study: the four methods considered presently in the SMAP ATBD for the  
321 passive-only product and three regression methods (described in Saleh et al (2006) and  
322 Mattar et al. (2012)) developed in the context of SMOS. The retrieved SM values were  
323 compared to a 'reference' SM data set obtained from the 2-P L-MEB inversion, which was  
324 assumed to be representative of the SM values over the ELBARA-II footprint. The seven SM  
325 retrieval approaches are described in the following sections. As is the case for the 2-P L-MEB  
326 method, these seven methods use the  $\tau$ - $\omega$  radiative transfer model (described above) to  
327 account for the vegetation effects and they all assume  $\tau_{NAD}$  is independent of polarization and  
328 incidence angle ( $\tau_V(0^\circ) = \tau_H(0^\circ) = \tau_{NAD}$ ). They are based on the same equation (1) to model  
329 the roughness effects, considering that  $N_{RV} = N_{RH} = 0$ . Furthermore, as implemented here they  
330 all use the 'Mironov' equations to compute the effective soil dielectric permittivity  $\epsilon_G$ . All of  
331 the parameters listed in Table 1 for the 2-P L-MEB method are accounted for in the seven SM  
332 retrieval methods considered. Only a very brief description of the SCA-H, SCA-V, DCA and  
333 LPRM methods will be given here as a detailed description of these methods is available in  
334 the initial release of the ATBD. All these four methods were applied to the ELBARA-II  $T_B$   
335 data at the incidence angle of  $40^\circ$  corresponding to the SMAP observations. A summary of  
336 the input variables required for the seven different retrieval methods, as well as for the  
337 reference algorithm 2-P L-MEB, is given in Table 2.

338

### 339 **2.4.1 Single Channel Algorithms (SCA-H and SCA-V).**

340 The Single Channel Algorithm (SCA-H), based on horizontally polarized  $T_B$  observations, is  
 341 the current SMAP baseline, but the same algorithm can also be applied to vertically polarized  
 342  $T_B$  data (SCA-V). In SCA-H, brightness temperatures are converted to emissivity using a  
 343 surrogate for the temperature of the emitting surface layer (in this study, the soil temperature  
 344 provided by ECMWF ( $T_{E-07}$ ) is used). The derived emissivity is corrected for vegetation and  
 345 surface roughness to obtain the soil emissivity. Finally, a dielectric mixing model (the  
 346 ‘Mironov’ model in this study) is used to obtain soil moisture SM from the soil dielectric  
 347 constant  $\epsilon_G$  using the Fresnel equations.

348 In this investigation, SCA-H and SCA-V are based on the same corrections of vegetation  
 349 (using the  $\tau$ - $\omega$  model), and soil roughness effects (using the  $H_R$  and  $Q_R$  parameters) as those  
 350 used for the 2-P L-MEB method.

351  $\tau_{NAD}$  is estimated from the vegetation water content (VWC) as

$$352 \quad \tau_{NAD} = b \cdot VWC \quad (7)$$

353 where  $b$  is a proportionality factor mainly depending on the vegetation structure.

354 For SMAP, values of  $b$  will be provided by means of a land cover look up table and the  
 355 baseline approach utilizes a set of land cover-based equations to estimate VWC from values  
 356 of NDVI. The following equation is used for cropland (O’Neill et al, 2013):

$$357 \quad VWC = (1.9134 \times NDVI^2 - 0.3215 \times NDVI) + \text{Stemfactor} \times (NDVI_{ref} - 0.1) / (1 - 0.1)$$

358 (8)

359 where Stemfactor parameter is the product of the average height of a land cover class and the  
 360 ratio of sapwood area to leaf area;  $NDVI_{ref}$  is assumed to be equal to the maximum value of  
 361 NDVI time series (the value of  $NDVI_{ref}$  was set equal here to 0.4696 from the analysis of the  
 362 MODIS NDVI observations over the 2010-2012 period). In this study, the  $b$  and Stemfactor  
 363 parameters were calibrated prior to the inversion process, as described in Section 2.5.

364

#### 365 2.4.2 The Dual Channel Algorithm (DCA)

366 The Dual Channel Algorithm (DCA) is an extension of the SCA and uses both H-polarized  
 367 and V-polarized  $T_B$  observations to simultaneously retrieve SM and VWC (O’Neill et al,  
 368 2013). As in the 2-P L-MEB algorithm, the SM and  $\tau_{NAD}$  variables are adjusted iteratively  
 369 until the root mean square difference between the simulated and observed  $T_B$  is minimized.  
 370 There are differences between 2-P L-MEB and DCA algorithms. Firstly,  $T_B$  data at  $\theta = 40^\circ$   
 371 are used for DCA, while multiangular data are used for 2-P L-MEB. Secondly, the  $ttv$

372 parameter (accounting for an angular dependence of  $\tau$ ) is retrieved in 2-P L-MEB, while DCA  
373 does not account for this dependence. Except for the  $tt_V$  and  $tt_H$  parameters, all vegetation and  
374 soil parameters used in DCA are the same as those used in the 2-P L-MEB method (Table 1).

375

#### 376 2.4.3 Land Parameter Retrieval Model (LPRM)

377 The LPRM approach uses an analytical solution for the derivation of the vegetation optical  
378 depth. This solution uses the Microwave Polarization Difference Index (MPDI) and the  
379 observed surface emissivity ( $\epsilon_H$  and  $\epsilon_V$ ) as input and is based on the assumption that the  
380 values of the vegetation optical depth are the same for both polarization ( $\tau_V = \tau_H$ ). The MPDI  
381 index is calculated from the brightness temperature at H- and V polarizations as follows  
382 (Meesters et al., 2005):

383

$$384 \quad \text{MPDI} = (T_{BV} - T_{BH}) / (T_{BV} + T_{BH}) \quad (8)$$

385

386 Then based on equation (4) of the  $\tau$ - $\omega$  omega model, soil moisture is retrieved using an  
387 optimization routine that minimizes the RMSE between the modelled and observed H-  
388 polarized brightness temperatures. As for SMOS, the vegetation optical depth at this  
389 optimized soil moisture value is an additional retrieval result. As noted in O'Neill et al.  
390 (2013), the LPRM was implemented on multifrequency satellites such as AMSR-E, where  
391 also the Ka-band V-polarized channel is used to retrieve physical temperatures of the scene  
392 observed. This latter can also be estimated from re-analysis or near real time data from  
393 weather prediction centres (Parinussa et al., 2011), as is done in the current SMOS SM  
394 retrieval algorithm (Kerr et al., 2012). Only a few studies (e.g. de Jeu et al., 2009) have  
395 examined the applicability of this model at L-band frequencies, although the analysis of  
396 SMOS data with LPRM is currently underway. All detailed equations of the LPRM approach  
397 are given in (Owe et al., 2001; Meesters et al., 2005, Owe et al., 2008, de Jeu et al., 2009,  
398 Chung et al., 2013). As for DCA, except for the  $tt_V$  and  $tt_H$  parameters which are not relevant  
399 here, all vegetation and soil parameters used in LPRM are the same as those used in the 2-P  
400 L-MEB method (Table 1).

401

#### 402 2.4.4 Linear regression methods (Saleh et al., 2006; Mattar et al., 2012)

403

404 Two methods based on regression equations developed by Saleh et al. (2006) and Mattar et al.  
 405 (2012) were evaluated in this study. Both methods were numerically derived from the  
 406 equations of the  $\tau$ - $\omega$  model assuming, as for LPRM, that the value of the effective scattering  
 407 albedo is  $\omega_p = 0$ , and that the values of optical depth  $\tau_p$  are the same for both polarizations  $p =$   
 408 H, V. These methods are physically-based. However, as the development of an analytical  
 409 formulation would be complex, most of the time they are used as regressions methods. As  
 410 shown by Saleh et al. (2006), a key interest in these regression methods is that they can be  
 411 used for varying roughness and vegetation conditions over time: no additional information  
 412 about temporal changes in these two state variables (such as NDVI or LAI for vegetation for  
 413 instance) is required. These regression methods have been used in several studies based on *in*  
 414 *situ*, airborne or spaceborne (SMOS) observations (Albergel et al., 2011; Parrens et al., 2012;  
 415 Calvet et al., 2011, etc.)

416 The method of Saleh et al. (2006) can be applied to observations made either at the two  
 417 incidence angles  $\theta_1$  and  $\theta_2$  (referred to as ‘Saleh’ bi-angular):

$$418 \quad \ln(\text{SM}) = a_2 \ln(\Gamma_p(\theta_1)) + a_1 \ln(\Gamma_p(\theta_2)) + a_0(\theta_1, \theta_2, p)$$

419 (9)

420 or to bi-polarization observations made at one observation angle  $\theta$  (referred to as ‘Saleh’ bi-  
 421 polarization):

$$422 \quad \ln(\text{SM}) = b_2 \ln(\Gamma_H(\theta)) + b_1 \ln(\Gamma_V(\theta)) + b_0(\theta)$$

423 (10)

424 where  $\Gamma_p(\theta)$  is the reflectivity of the soil-vegetation system at polarization  $p$  ( $p=V$  or  $p=H$ ),  
 425 defined as

$$426 \quad \Gamma_p(\theta) = 1 - T_{BP}(\theta) / T_{GC} \quad (11)$$

427 where the composite soil vegetation surface temperature  $T_{GC}$  was estimated from the ERA-  
 428 INTERIM 0-7cm soil temperature product ( $T_{E-07}$ ).

429 The method of Mattar et al. (2012) is very similar and can be written as (referred to as  
 430 ‘Mattar’):

$$431 \quad \ln(\text{SM}) = c_2 \ln(\Gamma_p(\theta)) + c_1 \text{NDVI} + c_0(\theta, p)$$

432 (12)

433 where the NDVI is considered here as a proxy for optical depth, as in the SCA-H and SCA-V  
 434 methods.



435 In the above equations (9), (10) and (12), the parameters ( $a_0, a_1, a_2$ ), ( $b_0, b_1, b_2$ ) and ( $c_0, c_1, c_2$ )  
436 are regression coefficients, which are assumed to be constant in time and have to be calibrated  
437 over each pixel. In this study, in the ‘Saleh bi-polarization’ equation (10), we used the  
438 observation angle  $\theta = 40^\circ$  as used in the other retrieval methods. In the ‘Saleh bi-angular’  
439 equation (9), we used H-polarized bi-angular observations at  $\theta_1 = 30^\circ$  and  $\theta_2 = 50^\circ$ . In the  
440 ‘Mattar’ equation (12), we used H-polarized observations at  $\theta = 40^\circ$ . These latter  
441 configurations were found to be the best for SM retrievals (results not shown here).

442

## 443 **2.5 Method calibration**

444 In this study, the SCA-V, SCA-H, DCA and LPRM methods were based on the L-MEB  
445 model parameters given in Table 1. In addition, some model parameters specific to some  
446 methods had to be calibrated. The DCA and LPRM methods did not require any additional  
447 calibration. Conversely, in the SCA-V and SCA-H methods, the two parameters  $b$  and  
448 Stemfactor, used to link NDVI and optical depth, had to be calibrated. Moreover, the three  
449 ‘regression’ methods ‘Saleh bi-angular’, ‘Saleh bi-polarization’ and ‘Mattar’ did not require  
450 any L-MEB parameters but required the calibration of three coefficients ( $a_i$ ), ( $b_i$ ) or ( $c_i$ ) ( $i = 0,$   
451  $1$  and  $2$ ) used in equations (8), (9) and (11), respectively.

452 The calibration of the above parameters and coefficients was performed three times, using one  
453 year of data for calibration and the two other years for validation. To calibrate the  $b$  and  
454 Stemfactor parameters in SCA-H and SCA-V, a multilinear regression method was used to fit  
455 the optical depth derived from equations (6) and (7) to the ‘reference’ optical depth  $\tau_{\text{NAD}}$   
456 retrieved from the 2-P L-MEB method. The obtained values for all three calibration years  
457 (2010, 2011 and 2012) are given in Table 3.

458 Similarly, to calibrate the three coefficients in the regression equations of the ‘Saleh bi-  
459 angular’, ‘Saleh bi-polarization’ and ‘Mattar’ methods, a multilinear regression method was  
460 used to minimize the difference between the retrieved SM derived from equations (9), (10) or  
461 (12) to the ‘reference’ SM values retrieved from the 2-P L-MEB method. The obtained values  
462 of the coefficients for all three methods and all three calibration years (2010, 2011 and 2012)  
463 are given in Table 3.

464

465

## 466 **3. Results**

467

### 468 **3.1. Reference values of SM and $\tau_{\text{NAD}}$**

469 As outlined above, the ‘reference’ values of soil moisture (SM) and optical depth at nadir  
470 ( $\tau_{\text{NAD}}$ ) were retrieved from the multiangular  $T_{\text{B}}$  data measured by the ELBARA-II instrument.  
471 The  $T_{\text{B}}$  measured  $\theta = 40^\circ$  for the time period 2010-2012 are shown in Fig. 2. A clear seasonal  
472 cycle in the  $T_{\text{B}}$  time-series can be seen, with maximum values of  $T_{\text{B}}$  during summer and lower  
473  $T_{\text{B}}$  values during winter. This annual cycle is related to the vegetation growth cycle,  
474 beginning in April and ending in November, and to the soil moisture conditions, which are  
475 generally drier during the summer period.

476 However, as already noted in Section 2.2, significantly wetter/drier conditions were  
477 encountered in 2010/2012, respectively, which is reflected in the observed  $T_{\text{B}}$  trends over the  
478 MELBEX-II site with lower values during summer 2010 compared to summer 2012. Based  
479 on these  $T_{\text{B}}$  observations, the retrieved values of SM and  $\tau_{\text{NAD}}$  were computed from the 2-P L-  
480 MEB method and they are illustrated in Fig. 3a-b. As discussed in Jackson et al. (2012),  
481 conditions of standing water during or shortly after intensive rainfalls should be flagged. In  
482 this study, to avoid these conditions, all retrieved values of SM which were found to be larger  
483 than the saturation value  $\text{SM}_{\text{SAT}}$  were not considered ( $\text{SM}_{\text{SAT}}$  was set equal to  $0.5 \text{ m}^3/\text{m}^3$  over  
484 the M-III site as computed by Juglea et al. (2010)). Note that due to this data filtering, the  
485 number of SM data used in the comparison may vary slightly from one approach to the other.

486 In accordance with the above-discussed  $T_{\text{B}}$  trends one can see that rainy conditions led  
487 generally to higher values of SM throughout the year in 2010 and during the winter period in  
488 2011 and 2012 (Fig. 3a). Drier conditions during the second half of 2011 and 2012 led to  
489 rather long time intervals of lower SM values.

490 The vegetation cycle could be clearly distinguished from the time variations in both the  
491 optical depth at nadir ( $\tau_{\text{NAD}}$ ) and NDVI index obtained over the 250 m MODIS pixel  
492 including the M-III vineyard (Fig. 3b). Relatively similar maximum values of  $\tau_{\text{NAD}}$  were  
493 retrieved during the summer of all three years (maximum values of  $\tau_{\text{NAD}}$  are close to 0.24 in  
494 2010 and close to 0.22 in 2011 and 2012). During the winter period, after vine pruning and  
495 defoliation, values of  $\tau_{\text{NAD}}$  close to 0.05 were retrieved for all three years. This latter value  
496 corresponds to the estimated value of the optical depth ( $\tau_{\text{STOCK}}$ ) of vine stocks (Schwank et

497 al., 2012; Wigneron et al., 2012). Superimposed on the long term trend of  $\tau_{\text{NAD}}$ , short-time  
498 changes in the time variations of  $\tau_{\text{NAD}}$  can be noted. It is likely that these apparent fluctuations  
499 result from unaccounted for changes in the roughness conditions over the field as discussed in  
500 Patton and Hornbuckle (2013) and Jackson et al. (2012) for SMOS observations. It can be  
501 noted too that very low values of  $\tau_{\text{NAD}}$  were retrieved during a short period of time in May of  
502 2011 and 2012, just before the vine vegetation growth. We assumed that this could be caused  
503 by specific effects during this period related to soil roughness or to vegetation structure. For  
504 instance, this effect could be linked to lower roughness conditions in relation to field works in  
505 May. As the roughness parameterization is set as constant over the 3 year period, actual lower  
506 roughness conditions in the field would lead to retrievals of lower  $\tau_{\text{NAD}}$  values and, to a lesser  
507 extent, higher SM values. Our field observations of roughness for the year 2012 (Fig. 1) are  
508 not accurate enough to confirm clearly this assumption but they seem to be leaning in that  
509 direction.

510 A maximum value of NDVI is reached in the middle of July ( $\sim$  DoY 200):  $\text{NDVI}_{\text{MAX}} \approx 0.45$   
511 in 2010 and 2011 and  $\text{NDVI}_{\text{MAX}} \approx 0.36$  in 2012. It is likely the lower value of  $\text{NDVI}_{\text{MAX}}$  in  
512 2012 can be related to the drier conditions during that year. In comparison with the year 2011,  
513 it seems that the very dry conditions during 2012 impact the NDVI values, but do not impact  
514 the time variations of  $\tau_{\text{NAD}}$  considerably.

515 A scatter plot of the retrieved values of the optical depth  $\tau_{\text{NAD}}$  versus the NDVI index is  
516 shown in Fig. 4. It can be seen that the results are generally consistent from one year to the  
517 other. One specific pattern can be noted in 2011; it corresponds to very low values of  $\tau_{\text{NAD}}$   
518 retrieved while vegetation is fully developed ( $\text{NDVI} \approx 0.45$ ), which was already discussed  
519 above.

520

### 521 **3.3 Comparison of SM Retrievals**

522 The retrieved values of SM from all retrieval methods presented in section 2 were compared  
523 to the reference SM values retrieved with the 2-P L-MEB method applied to the  
524 measurements performed during the years 2010-2012. A summary of this comparison is given  
525 in Table 4, in terms of coefficient of determination ( $R^2$ ), bias ( $\text{m}^3/\text{m}^3$ ), RMSE ( $\text{m}^3/\text{m}^3$ ) and  
526 unbiased RMSE (ubRMSE,  $\text{m}^3/\text{m}^3$ ) as defined by Entekhabi et al. (2010). To illustrate the

527 results, scatter plots of retrieved SM values versus ‘reference’ SM values are given for all  
528 methods considered in this study (Fig. 5).

529 All five methods requiring a calibration step, e.g. SCA-V, SCA-H, ‘Saleh’ bi-angular, ‘Saleh’  
530 bi-polarization and ‘Mattar’ (the calibration was made using one year and the evaluation with  
531 the two other years), provided SM retrievals that were in good agreement with the ‘reference’  
532 SM data ( $R^2$  is generally higher than 0.90, and the RMSE is lower than  $0.045 \text{ m}^3/\text{m}^3$ ). If we  
533 consider the years used for calibration, best performances in terms of  $R^2$  for all four methods  
534 were obtained when year 2010 (corresponding to rather ‘wet’ conditions) was used for  
535 calibration, while lower performances were obtained using the year 2012 (corresponding to  
536 ‘very dry’ conditions) for calibration. Results for the year 2011 are generally close to those  
537 obtained for the year 2010. A closer inspection shows that both the SCA-V and the SCA-H  
538 methods provide generally very similar performances in SM retrievals (the SCA-V method  
539 providing a slightly better accuracy in terms of  $R^2$ , bias, RMSE and ubRMSE). The three  
540 methods based on regression equations (‘Saleh’ bi-polarization, ‘Saleh’ bi-angular, and  
541 ‘Mattar’) provided very similar results too. Slightly lower performances were obtained for the  
542 ‘Mattar’ method (especially when using the year 2010 for calibration), while best  
543 performances were obtained for ‘Saleh bi-angular’. Considering the ubRMSE criteria, the  
544 performances of the SCA and the regression methods were even closer. Except for the DCA  
545 and LPRM algorithm, the ubRMSE is always around or below the target accuracy for SMAP  
546 of  $0.04 \text{ m}^3/\text{m}^3$ . This is a direct consequence of the fact that values of the bias were found to be  
547 higher for the SCA methods (bias  $\approx 0.020 \text{ m}^3/\text{m}^3$ ) than for the regression methods (bias  $\approx$   
548  $0.010 \text{ m}^3/\text{m}^3$ ).

549 As could be expected, results obtained from methods which did not require parameter  
550 calibration (DCA and LPRM) provided results with a lower accuracy: the RMSE was similar  
551 for both methods (RMSE  $\approx 0.55 \text{ m}^3/\text{m}^3$ ), while slightly better  $R^2$  values were obtained for  
552 DCA ( $R^2 = 0.79$ ) than for LPRM ( $R^2 = 0.725$ ). For both methods, the bias in the retrievals  
553 was found to be very low (bias =  $0.021 \text{ m}^3/\text{m}^3$  for DCA, and bias =  $0.013 \text{ m}^3/\text{m}^3$  for LPRM).

554 The scatter plots (Fig. 5) showing the comparison between retrieved SM values versus  
555 ‘reference’ SM values are given to illustrate these different results. For methods requiring  
556 calibration (SCA-V, SCA-H, ‘Saleh’ bi-angular, ‘Saleh’ bi-polarization and ‘Mattar’), we  
557 used the year 2010 in Fig. 5 (this year provided best performances in terms of  $R^2$ ). Note that

558 the number of data used in the comparison may vary from one approach to the other. This can  
559 be explained by two reasons. First, for DCA and LPRM, the comparison was made over three  
560 years (2010 - 2012), while it was made over two years (2011 -2012) for the other methods.  
561 Second, retrieved SM values larger than the saturation value  $SM_{SAT}$  ( $SM_{SAT} = 0.5 \text{ m}^3/\text{m}^3$ )  
562 were removed in the comparison (a very low number of observations was concerned by this  
563 filtering).

564 It can be seen that a very low bias was obtained generally. However, in wet conditions, the  
565 methods LPRM and DCA provided underestimated SM values (for  $SM > 0.3 \text{ m}^3/\text{m}^3$ ); while  
566 the ‘Saleh’ and ‘Mattar’ methods provided overestimated SM values (for  $SM > 0.2 \text{ m}^3/\text{m}^3$ )  
567 with respect to the reference SM. For DCA and LPRM (methods with do not require any  
568 calibration), it can be seen that the SM retrieval performances are lower in a small SM  
569 interval, for values of SM comprised between  $\sim 0.1$  and  $0.15 \text{ m}^3/\text{m}^3$ . These SM conditions  
570 generally correspond to periods of vegetation growth at the end of spring and of full  
571 vegetation development in the summer period.

572

#### 573 **4. Discussion and conclusion**

574 This study presents an inter-comparison of several SM retrieval methods based on a three year  
575 data set of passive L-band microwave observations acquired over a vineyard site at the VAS  
576 site.

577 A careful interpretation of the results should be made, and the results cannot be easily  
578 generalized to operational applications for spaceborne sensors. We will discuss these different  
579 aspects and the main conclusions of the study in the following. First, it is important to  
580 consider that the results were obtained at the field scale and over only one type of vegetation  
581 (a vineyard canopy) with some specific features (no litter layer, relatively low LAI and  
582 biomass conditions, frequent agricultural practices leading to changes in soil roughness, etc.).  
583 Several effects related to changes in the soil roughness conditions or in the vegetation  
584 structure (in relation with the crop growth and the agricultural practices) may have a  
585 significant impact on the results of the present study. It is likely that the impact of these  
586 effects would average out and, therefore, become much less important if we had considered  
587 larger footprints of spaceborne radiometric observations, including a large variety in the types  
588 of vegetation (natural or cultivated canopies), in the soil conditions and in the agricultural

589 practices. For instance, specific effects related to the vegetation structure could be revealed  
590 over the vineyard field and the values of optical depth for both polarizations ( $\tau_H(\theta)$  and  $\tau_V(\theta)$ )  
591 could not be considered as equal for that canopy type (Wigneron et al., 2012). This result has  
592 frequently been obtained from *in situ* radiometric observations (Pardé et al., 2003, 2004;  
593 Wigneron et al., 2004) but it has never been noted, to our knowledge, from spaceborne  
594 observations. For instance, Owe et al. (2001) found that  $\tau_V = \tau_H$  over test sites in the US over  
595 a variety of land covers based on SMMR (Scanning Multichannel Microwave Radiometer)  
596 observations at C-band. It is likely that these vegetation structure effects can be a limitation  
597 for presented evaluation of the methods, which all assume  $\tau_H = \tau_V$ . So, several similar studies  
598 based on *in situ* observations over a variety of vegetation types are required to provide a more  
599 in-depth evaluation of the method performances.

600 It should be noted too that the performances of the different methods cannot be compared  
601 directly as some methods had to be calibrated while some methods did not require any  
602 parameter calibration step (DCA and LRPM). The two methods SCA-H and SCA-V, require  
603 the calibration of the relationship between optical depth and a remotely sensed vegetation  
604 index (NDVI); the three methods based on regression equations, ‘Saleh bi-angular’, ‘Saleh bi-  
605 polarization’ and ‘Mattar’, require the calibration of three coefficients. This calibration step  
606 could be done in the present study as we considered that a ‘reference’ data set describing the  
607 time variations in SM and  $\tau_{NAD}$  (and derived from multi-angular observations) was available  
608 from the ELBARA-II tower-based observations. However, for operational spatial  
609 applications, it is generally very difficult to obtain such a reference data set.

610 In spite of the limitations discussed above, some key results obtained in this study from  
611 tower-based observations could be of value to future operational applications. It was found  
612 that the two methods, which did not require any a priori calibration (DCA and LRPM) could  
613 provide good SM retrievals and have relatively similar performances ( $R^2 \sim 0.72-0.79$ ;  
614  $RMSE \sim 0.054-0.58 \text{ m}^3/\text{m}^3$ ) over the three year period. The methods requiring parameter  
615 calibration (two parameters in SCA-H and SCA-V; three coefficients in the three regression  
616 methods) provided results closer to the reference: for instance the  $R^2$  coefficient increased  
617 generally to values larger than 0.90 for all methods. The methods which require additional  
618 information concerning the vegetation development (the NDVI variable is required in the  
619 SCA-H, SCA-V and ‘Mattar’ algorithms) provided slightly lower performances when year  
620 2012 was used for calibration. For that year the NDVI values were lower than for the two



621 other years (maximum NDVI values  $\approx 0.45$  in 2010 and 2011 and  $\approx 0.36$  in 2012), while the  
622 maximum values of  $\tau_{\text{NAD}}$  were found to be relatively similar over all three years ( $\approx 0.22 -$   
623  $0.24$ ). It is likely that nonlinearities between  $\tau_{\text{NAD}}$  and NDVI led to these slightly lower  
624 performances in SM retrievals for the year 2012 for the SCA and ‘Mattar’ algorithms.

625 In the present study, the computed performances are “optimal” performances as it is assumed  
626 that a good parameter calibration can be made from a SM data set which can be considered as  
627 a reference. This calibration step was possible in this study based on *in situ* tower-based  
628 observations obtained over a homogeneous vineyard field, but this step is much more  
629 complex for operational applications based on space borne sensors. Several options are  
630 possible to calibrate these different retrieval methods for spaceborne applications. For  
631 instance, the reference SM or  $\tau_{\text{NAD}}$  values which are required in the calibration step can be  
632 estimated:

633 (i) from networks of *in situ* measurement sites such as SCAN in the USA (Schaefer et al.,  
634 2007), OZNET in Australia (Smith et al., 2012) or SMOSMANIA in France (Albergel et al.,  
635 2012), etc. Then, based on results obtained over a variety of soil and vegetation conditions, a  
636 look up table providing the calibrated parameters as function of the land cover types can be  
637 built.

638 (ii) from model re-analyses (ERA-Interim (Dee et al., 2011) or MERRA Land (Reichle et al.,  
639 2012) for instance), in regions where the simulated SM values can be considered to be  
640 accurate. As mentioned above, in a second step, a look up table can be built for a variety of  
641 land covers.

642 (iii) by combining observations from different remote sensing sensors. For instance, the  
643 estimation of optical depth  $\tau_{\text{NAD}}$  retrieved from SMOS or other satellites (e.g. AMSR-2) could  
644 be used to calibrate the vegetation parameters required in the SCA-H and SCA-V algorithms  
645 (Lawrence et al., 2014).

646 Future work will consider these different options to evaluate the retrieval capabilities of the  
647 different methods requiring calibration (SCA, ‘Saleh’ or Mattar’) for operational applications  
648 based on spaceborne sensors.

649

650

651 **Acknowledgments**

652

653 This study received financial support from the TOSCA program of CNES (Centre National  
654 d'Etudes Spatiales, France), the Spanish National Program on Space Research (MIDAS-5 and -  
655 6 Projects) and ESA (European Space Agency) in the framework of the cal/val activities of  
656 the SMOS mission. The MODIS MOD13Q1 data were obtained through the online Data Pool  
657 at the NASA Land Processes Distributed Active Archive Center (LP DAAC), USGS/Earth  
658 Resources Observation and Science (EROS) Center, Sioux Falls, South Dakota  
659 ([http://lpdaac.usgs.gov/get\\_data](http://lpdaac.usgs.gov/get_data)). The CATDS data were obtained from the "Centre Aval de  
660 Traitement des Données SMOS" (CATDS), operated for the "Centre National d'Etudes  
661 Spatiales" (CNES, France) by IFREMER (Brest, France).

662

663 **References**

- 664 Albergel, C., Zakharova, E., Calvet, J.-C., Zribi, M., Pardé, M., Wigneron, J.-P., Novello, N.,  
665 Kerr, Y., Mialon, A., Fritz, N. (2011). A first assessment of the SMOS data in southwestern  
666 France using *in situ* and airborne soil moisture estimates: the CAROLS airborne campaign.  
667 *Remote Sensing of Environment*, 115, 2718-2728.
- 668 Al Bitar, A., Leroux, D., Kerr, Y. H., Merlin, O., Richaume, P., Sahoo, A., Wood, E. F.  
669 (2012). Evaluation of SMOS Soil Moisture products over continental US using the  
670 SCAN/SNOTEL network. *IEEE Transactions on Geoscience and Remote Sensing*. 50(5),  
671 1572 – 1586.
- 672 Berthon, L., Mialon, A., Al Bitar, A., Cabot, F. and Kerr, Y.H. (2012). SMOS CATDS Level  
673 3 Soil Moisture Products. *Proceedings of 2012 EGU General Assembly*, Vienna, April 2012.
- 674 Bindlish, R., Jackson, T., Cosh, M., Zhao, T. & O’Neill, P. (2014). Global Soil Moisture from  
675 the Aquarius Satellite: Description and Initial Assessment. *IEEE Geoscience and Remote*  
676 *Sensing Letters*, submitted.
- 677 De Lannoy, G. J. M., Reichle, R. H. & Pauwels, V. R. N. (2013). Global Calibration of the  
678 GEOS-5 L-Band Microwave Radiative Transfer Model over Nonfrozen Land Using SMOS  
679 Observations. *Journal of Hydrometeorology*, 14, 765-785.
- 680 Calvet, J.-C., Wigneron, J.-P., Walker, J., Karbou, F., Chanzy, A. & Albergel, C. (2011).  
681 Sensitivity of passive microwave observations to soil moisture and vegetation water content:  
682 from L-band to W-band. *IEEE Transactions on Geoscience and Remote Sensing*. 49, 4, 1190-  
683 1199.
- 684 Cano A., Saleh, K., Wigneron, J.-P., Antolín, C., Balling, J. E., Kerr, Y. H., Kruszewski, A.,  
685 Millán-Scheiding, C., Schmidl Søjbjerg, S., Skou, N., López-Baeza, E. (2010). The SMOS  
686 Mediterranean Ecosystem L-Band characterisation EXperiment (MELBEX-I) over natural  
687 shrubs, *Remote Sensing of Environment*, 114(4), 844-853.
- 688 Chung, D., de Jeu, R.A.M., Dorigo, W., Hahn, S., Melzer, T., Parinussa R.M. et al. (2013).  
689 ESA CCI soil moisture algorithm theoretical baseline document version 1, pp. 36–44.  
690 <http://www.esa-soilmoisture-cci.org/>

691 Dee, D. P., Uppala, S. M., Simmons, A. J., Berrisford, P., Poli, P., Kobayashi, S., et al.  
692 (2011), The ERA-Interim reanalysis: configuration and performance of the data assimilation  
693 system, *Quarterly Journal of the Royal Meteorological Society*, 137, 553–597.  
694 doi: 10.1002/qj.828.

695 de Jeu, R., Holmes, T., Panciera, R. & Walker, J. (2009). Parameterization of the Land  
696 Parameter Retrieval Model for L-Band Observations Using the NAFE'05 Data Set. *IEEE*  
697 *Geoscience and Remote Sensing Letters*, 6 (4), 630-634.

698 de Rosnay P., Calvet, J.-C. , Kerr, Y., Wigneron, J.-P., Lemaître, F. et al. (2006). SMOSREX:  
699 A Long Term Field Campaign Experiment for Soil Moisture and Land Surface Processes  
700 Remote Sensing. *Remote Sensing of Environment*, 102, 377-389.

701 Dobson, M. C., Ulaby, F. T., Hallikainen, M. T., & El-Reyes, M. A. (1985). Microwave  
702 dielectric behavior of wet soil- Part II: Dielectric mixing models. *IEEE Transactions on*  
703 *Geoscience and Remote Sensing.*, 23, 35-46.

704 Entekhabi, D., Reichl, R. H., Koster R. D., Crow, W. T. (2010). Performance Metrics for Soil  
705 Moisture Retrievals and Application Requirements. *Journal of Hydrometeorology*, 11, 832-  
706 840.

707 Entekhabi, D., Njoku, E., O'Neill, P., Kellogg, K. et al. (2010). The Soil Moisture Active  
708 Passive (SMAP) Mission. *Proceedings of the IEEE*, 98, 5.

709 Grant, J.P., Saleh, K., Wigneron, J.-P., Guglielmetti, M., Kerr, Y., Schwank, M., Skou, N. &  
710 Van de Griend, A.A. (2008). Calibration of the L-MEB model over a coniferous and a  
711 deciduous forest. *IEEE Transactions on Geoscience and Remote Sensing*, 46(3), 808-818.

712 Hornbuckle, B K. & England, A. W. (2004). Radiometric Sensitivity to Soil Moisture at 1.4  
713 GHz Through a Corn Crop at Maximum Biomass. *Water Resources Research*, 40(10): doi:  
714 10.1029/2003WR002931.

715 Jackson, T. J., & Schmugge, T. J. (1991). Vegetation effects on the microwave emission of  
716 soils. *Remote Sensing of Environment*, 36, 203-212.

717 Jackson, T. J., Le Vine, D. M., Swift, C. T., Schmugge, T. J., & Schiebe, F. R. (1995).  
718 Large area mapping of soil moisture using the ESTAR passive microwave radiometer in  
719 Washita'92. *Remote Sensing of Environment*, 53, 27-37.

720 Jackson, T. J., Bindlish, R., Cosh, M. H., Zhao, T., Starks, P. J., Bosch, D. D., Seyfried, M. S.,  
721 Moran, M. S., Kerr, Y., & Leroux, D. (2012). Validation of Soil Moisture and Ocean Salinity  
722 (SMOS) soil moisture over watershed networks in the U.S. *IEEE Transactions on Geoscience  
723 and Remote Sensing*, 50, 5, 1530-1543.

724 Juglea, S., Kerr, Y., Mialon, A. Wigneron, J.-P., Lopez-Baeza, E., et al. (2010). Modelling  
725 soil moisture at SMOS scale by use of a SVAT model over the Valencia Anchor Station.  
726 *Hydrol. Earth Syst. Sci.*, doi:10.5194/hess-14-831-2010, 14, 831-846.

727 Kerr, Y. H., Waldteufel, P., Wigneron, J.-P., Font, J., & Berger, M., (2001). Soil Moisture  
728 Retrieval from Space: The Soil Moisture and Ocean Salinity (SMOS) Mission. *IEEE  
729 Transactions on Geoscience and Remote Sensing*, 39(8), 1729-1735.

730 Kerr Y. H., Waldteufel, P., Richaume, P., Wigneron, J.-P. et al. (2012). The SMOS soil  
731 moisture retrieval algorithm', *IEEE Transactions on Geoscience and Remote Sensing*, 50(5),  
732 1384-1403.

733 Kurum, M., Lang, R. H., O'Neill, P. E., Joseph, A. T., Jackson, T. J. , & Cosh, M. H. (2009).  
734 L-Band Radar Estimation of Forest Attenuation for Active/Passive Soil Moisture Inversion.  
735 *IEEE Transactions on Geoscience and Remote Sensing*, 47, 9, 3026-3040.

736 Kurum, M. (2013). Quantifying scattering albedo in microwave emission of vegetated terrain.  
737 *Remote Sensing of Environment*, 129, 66-74.

738 Lawrence, H., Wigneron, J-P, Demontoux, F., Mialon, A., & Kerr, Y. H. (2013). Evaluating  
739 the semi-empirical H – Q model used to calculate the emissivity of a rough bare soil, with a  
740 numerical modelling approach. *IEEE Transactions on Geoscience and Remote Sensing*, 51, 7,  
741 4075-4084.

742 Lawrence H., Wigneron, J.-P., Lopez-Baeza, E. et al. (2014). Comparison between SMOS  
743 Vegetation Optical Depth products and MODIS Vegetation Indices over the USA. *Remote  
744 Sensing of Environment*, 140, 396 – 406, 2014.

745 Le Vine, D. M., Lagerloef, G. S., & Torrusio, S. E. (2010). Aquarius and remote sensing of  
746 sea surface salinity from space. *Proceedings of the IEEE*, 98(5), 688-703.

747 Liu, S. F., Liou, Y.-A., Wang, W. J. Wigneron, J.-P. & Lee, J. B. (2002). Retrieval of crop  
748 biomass and soil moisture from measured 1.4 and 10.65 brightness temperatures. *IEEE*  
749 *Transactions on Geoscience and Remote Sensing*, 40(6), 1260-1268.

750 Luo, Y., Feng, X., Houser, P., Anantharaj, V., Fan, X. , De Lannoy, G. et al. (2013). Potential  
751 soil moisture products from the aquarius radiometer and scatterometer using an observing  
752 system simulation experiment. *Geosci. Instrum. Method. Data Syst.*, 2, 113–120.

753 Mattar, C., Wigneron, J.-P., Sobrino, J. A., Novello, N., Calvet, J.-C., Albergel, C.,  
754 Richaume, P., Mialon, A., Guyon, D., Jiménez Muñoz, J.C. & Kerr, Y. (2012). A combined  
755 optical-microwave method to retrieve soil moisture over vegetated areas. *IEEE Transactions*  
756 *on Geoscience and Remote Sensing*, 50(5), 1404-1413.

757 Meesters, A. G. C. A., de Jeu, R. A. M. et al. (2005). Analytical derivation of the vegetation  
758 optical depth from the microwave polarization difference index. *Geoscience and Remote*  
759 *Sensing Letters*, 2(2), 121-123.

760 Mialon, A., de Rosnay, P., Wigneron, J.-P., Escorihuela, M.-J. & Kerr, Y. H. (2012).  
761 Evaluating the L-MEB model from long term microwave measurements over a rough field,  
762 SMOSREX 2006. *IEEE Transactions on Geoscience and Remote Sensing*, 50(5), 1458-1467.

763 Mialon A., Al Bitar, A., Berthon, L. et al. (2012). Validation of SMOS Level 3 soil moisture',  
764 *IEEE International Geoscience and Remote Sensing Symposium, IGARSS'2012*, 22-27 July  
765 2012, Munich, Germany.

766 Mo, T., Choudhury, B.J., Schmugge, T.J., Wang J.R., & Jackson, T.J. (1982). A model for  
767 microwave emission from vegetation-covered fields. *J. of Geophysical Research*, 87,  
768 11.229-11.237.

769 MODIS (2010). NASA Land Processes Distributed Active Archive Center (LP DAAC).  
770 MOD13Q1 collection 5. USGS/Earth Resources Observation and Science (EROS) Center,  
771 Sioux Falls, South Dakota.

772 Njoku, E.G., Jackson, T.J., Lakshmi, V., Chan, T.K. & Nghiem, S.V. (2003). Soil moisture  
773 retrieval from AMSR-E. *IEEE Transactions on Geoscience and Remote Sensing*, 41(.2), 215-  
774 229.



775 O'Neill, P., Chan, S., Njoku, E., Jackson, T. & Bindlish R., Soil Moisture Active Passive  
776 (SMAP) Algorithm Theoretical Basis Document (ATBD), SMAP Level 2 & 3 Soil Moisture  
777 (Passive), (L2\_SM\_P, L3\_SM\_P), Initial Release, v.1,  
778 [http://smap.jpl.nasa.gov/files/smap2/L2&3\\_SM\\_P\\_InitRel\\_v1\\_filt2.pdf](http://smap.jpl.nasa.gov/files/smap2/L2&3_SM_P_InitRel_v1_filt2.pdf)

779 Owe, M., de Jeu, R., & Holmes, T. (2008). Multisensor historical climatology of satellite-  
780 derived global land surface moisture. *Journal of Geophysical Research-Earth Surface*, 113,  
781 F01002

782 Panciera, R., Walker, J. P., Kalma, J. D., Kim, E. J., Saleh, K., & Wigneron, J.-P. (2009).  
783 Evaluation of the SMOS L-MEB passive microwave soil moisture retrieval algorithm. *Remote*  
784 *Sensing of Environment*, 113, 435–444.

785 Pardé, M., Wigneron, J.-P., Chanzy, A., Waldteufel, P., Kerr, Y. & Huet, S. (2003). Retrieving  
786 surface soil moisture over a wheat field: Comparison of different methods. *Remote Sensing of*  
787 *Environment*, 87, 334-344.

788 Pardé, M, Wigneron, J-P, Chanzy, A., Kerr, Y., Calvet, J.C., Waldteufel, P., Schmidl, S. &  
789 Skou, N. (2004). N-Parameter retrievals from L-band microwave measurements over a variety  
790 of agricultural crops, *IEEE Transactions on Geoscience and Remote Sensing*, 42(6), 1168-  
791 1178.

792 Parinussa, R. M., Holmes, T. R. H., Yilmaz, M. T. & Crow, W. T. (2011). The impact of land  
793 surface temperature on soil moisture anomaly detection from passive microwave  
794 observations. *Hydrol. Earth Syst. Sci.*, 15, 3135–3151.

795 Parrens, M., Zakharova, E., Lafont, S., Calvet, J.-C., Kerr, Y., Wagner, W., & Wigneron, J.-  
796 P. (2012). Comparing soil moisture retrievals from SMOS and ASCAT over France. *Hydrol.*  
797 *Earth Syst. Sci.*, 16, 423-440, doi:10.5194/hess-16-423-2012.

798 Pellarin, T., Mialon, A., Biron, R. et al. (2013). Two years of L-band radiometry over a  
799 mountainous region: topography, snow and freezing soil issues. *IEEE International Geoscience*  
800 *and Remote Sensing Symposium*, IGARSS 2013, 21-26 July, Melbourne.

801 Rodriguez-Fernandez, NJ, Aires, F, Richaume, P, Prigent, C, & Kerr, Y.H. “Soil Moisture  
802 retrieval from SMOS observations using neural networks”, 2013, *to be submitted*

803 Reichle, R. H., Koster, R. D., De Lannoy, G. J. M., et al. (2011). Assessment and  
804 enhancement of MERRA land surface hydrology estimates, *J. Climate*, 24, 6322-6338,  
805 doi:10.1175/JCLI-D-10-05033.1.

806 Saleh, K., Wigneron, J.-P., de Rosnay, P., Calvet, J.-C. & Kerr, Y. (2006). Semi-empirical  
807 regressions at L-band applied to surface soil moisture retrievals over grass, *Remote Sensing of*  
808 *Environment*, 101, 415-426.

809 Schaefer, G. L., Cosh, M. H., and Jackson, T. J. (2007). The USDA Natural Resources  
810 Conservation Service Soil Climate Analysis Network (SCAN). *Journal of Atmospheric and*  
811 *Oceanic Technology*, 24(12), 2073-2077.

812 Schlenz, F., Fallmann, J., Marzahn, P., Loew, A. & Mauser, M. (2012). Characterization of  
813 Rape Field Microwave Emission and Implications to Surface Soil Moisture Retrievals.  
814 *Remote Sensing*, 4, 247-270; doi:10.3390/rs4010247.

815 Schwank, M., Wiesmann, A. et al. (2010). "ELBARA II, An L-Band Radiometer System for  
816 Soil Moisture Research. *Sensors*, MDPI 10: 584-612.

817 Schwank M, Wigneron, J.-P., Lopez-Baeza, E., Völksch, I., Mätzler, C. & Kerr, Y. (2012). 'L-  
818 Band Radiative Properties of Vine Vegetation at the MELBEX III SMOS Cal/Val Site. *IEEE*  
819 *Transactions on Geoscience and Remote Sensing*, 50(5), 1587-1601.

820 Smith, A. B., Walker, J. P., Western, A. W., Young, R. I., Ellett, K. M., Pipunic, R., Grayson,  
821 R., Siriwidena, L., Chiew, F., and Richter, H. (2012). The Murrumbidgee soil moisture  
822 monitoring network data set. *Water Resources Research*, 48, W07701.1-6.

823 Wigneron, J. -P., Chanzy, A., Calvet, J. -C., & Bruguier, N. (1995). A simple algorithm to  
824 retrieve soil moisture and vegetation biomass using passive microwave measurements over  
825 crop fields. *Remote Sensing of Environment*, 51(3), 331-341.

826 Wigneron, J.-P., Waldteufel, P., Chanzy, A., Calvet, J.-C., & Kerr, Y. (2000). Two-D  
827 microwave interferometer retrieval capabilities of over land surfaces (SMOS Mission).  
828 *Remote Sens. Environ.*, 73, 270-282.

829 Wigneron J.-P., Calvet, J.-C., de Rosnay, P., Kerr, Y., Waldteufel, P., Saleh, K. et al. (2004).  
830 Soil Moisture Retrievals from Bi-Angular L-band Passive Microwave Observations. *IEEE*  
831 *Trans. Geosc. Remote Sens. Let.*, 1(4), 277-281.

832 Wigneron, J.-P., Kerr, Y., Waldteufel, P., Saleh, K., Escorihuela, M.-J., Richaume, P.,  
833 Ferrazzoli, P., de Rosnay, P., Gurney, R., Calvet, J.-C., Guglielmetti, M., Hornbuckle, B.,  
834 Matzler, C., Pellarin, T., & Schwank, M. (2007). L-band Microwave Emission of the  
835 Biosphere (L-MEB) Model: description and calibration against experimental data sets over  
836 crop fields. *Remote Sensing of Environment*, *107*(4), 639–655.

837 Wigneron, J-P, Schwank, M., Lopez Baeza, E., et al. (2012). First evaluation of the SMOS  
838 observations over the VAS site in the Mediterranean region. *Remote Sensing of Environment*,  
839 *124*, 26–37.

840

841

842 **Table 1.**

843 L-MEB soil and vegetation parameters over the M-III vineyard (VAS site). All these parameters,  
844 except  $tt_H$  and  $tt_V$  which are specific to L-MEB, are valid for the other SM retrieval methods.

	Unit	Value or used Model
Soil dielectric permittivity ( $\epsilon_G$ )	(-)	Mironov et al. (2012)
Clay fraction	(-)	0.26 (in situ measurements; Juglea et al., 2010)
$T_G=T_C=T_{GC}$	K	ECMWF ERA Interim temperature ( $T_{E-07}$ )
$H_R$	(-)	0.6060 (calibrated, Lawrence et al., 2013)
$Q_R$	(-)	0.0303 (calibrated, Lawrence et al., 2013)
$N_{RH}$	(-)	0
$N_{RV}$	(-)	0
$tt_H$	(-)	1
$tt_V$	(-)	Free parameter in the retrieval process
$\omega$	(-)	0.02
$\tau$	(-)	Free parameter in the retrieval process
SM	$m^3/m^3$	Free parameter in the retrieval process

845

846

847 **Table 2.**

848 Input variables required in the different retrieval algorithms

849

<b>Algorithm</b>	<b>Input variables</b>
<b>SCA-H</b>	$T_{BH}(\theta=40^\circ)$ ECMWF temperature ( $T_{E-07}$ ) NDVI
<b>SCA-V</b>	$T_{BV}(\theta=40^\circ)$ ECMWF temperature ( $T_{E-07}$ ) NDVI
<b>DCA</b>	$T_{BH}(\theta=40^\circ)$ , $T_{BV}(\theta=40^\circ)$ ECMWF temperature ( $T_{E-07}$ )
<b>LPRM</b>	$T_{BH}(\theta=40^\circ)$ , $T_{BV}(\theta=40^\circ)$ ECMWF temperature ( $T_{E-07}$ )
<b>‘Saleh’ bi-polarization</b>	$T_{BH}(\theta=40^\circ)$ , $T_{BV}(\theta=40^\circ)$ ECMWF temperature ( $T_{E-07}$ )
<b>‘Saleh’, bi-angular</b>	$T_{BH}(\theta=30^\circ)$ , $T_{BH}(\theta=50^\circ)$ ECMWF temperature ( $T_{E-07}$ )
<b>‘Mattar’</b>	$T_{BH}(\theta=40^\circ)$ ECMWF temperature ( $T_{E-07}$ ) NDVI

850

851

852

853 **Table 3.**

854 Calibrated parameters of the different retrieval algorithms: one year (2010, 2011 or 2012) is used for  
855 calibration; the two other years are used for validation

856 **SCA H/V**,  $T_{BH}(\theta=40)$  or  $T_{BV}(\theta=40)$

Calibration	b	Stemfactor
2010	0.61679	0.20874
2011	0.31756	0.44014
2012	0.92819	0.05840

857 **'Saleh bi-angular'**,  $T_{BH}(\theta=30)$ ,  $T_{BH}(\theta=50)$

Calibration	$a_0$	$a_1$	$a_2$
2010	1.4171	-0.3560	0.8374
2011	1.0972	-0.2806	0.2613
2012	2.2857	-1.5674	0.1300

858

859 **'Saleh bi-polarization'**,  $T_{BH}(\theta=40)$ ,  $T_{BV}(\theta=40)$

Calibration	$b_0$	$b_1$	$b_2$
2010	0.3524	0.7734	1.1401
2011	0.2595	0.6208	0.4879
2012	-0.3914	1.1927	0.7263

860 **'Mattar'**,  $T_{BH}(\theta=40)$

Calibration	$c_0$	$c_1$	$C_2$
2010	1.2530	0.9491	0.9147
2011	0.9844	0.5748	0.3702
2012	1.0954	2.6578	0.0183

861

862

863

864 **Table 4.**

865 Performances of the different SM retrieval algorithms in terms of coefficient of determination ( $R^2$ ),  
 866 bias ( $m^3/m^3$ ), RMSE ( $m^3/m^3$ ) and ubRMSE ( $m^3/m^3$ ). For SCA-H, SCA-V, ‘Saleh bi-angular’, ‘Saleh  
 867 bi-polarization’ and ‘Mattar’, one year (2010, 2011 or 2012) is used for calibration; the two others are  
 868 used for validation. For LPRM and DCA, no calibration is required.

869

Method	Calibration	Validation	$R^2$	Bias ( $m^3/m^3$ )	RMSE ( $m^3/m^3$ )	ubRMSE ( $m^3/m^3$ )
SCA-H	2010	2011, 2012	0.915	-0.025	0.050	0.043
	2011	2010, 2012	0.905	-0.041	0.054	0.035
	2012	2010, 2011	0.852	-0.020	0.056	0.052
SCA-V	2010	2011, 2012	0.928	-0.014	0.035	0.032
	2011	2010, 2012	0.919	-0.024	0.040	0.032
	2012	2010, 2011	0.861	-0.010	0.045	0.043
DCA			0.789	0.021	0.054	0.050
LPRM			0.725	0.013	0.058	0.056
Saleh Bi-angular	2010	2011, 2012	0.950	0.004	0.037	0.037
	2011	2010, 2012	0.941	0.007	0.028	0.027
	2012	2010, 2011	0.934	0.009	0.036	0.035
Saleh Bi- polarization	2010	2011, 2012	0.946	0.010	0.040	0.039
	2011	2010, 2012	0.924	-0.001	0.031	0.031
	2012	2010, 2011	0.920	0.004	0.033	0.033
Mattar	2010	2011, 2012	0.946	0.009	0.041	0.040
	2011	2010, 2012	0.927	-0.001	0.030	0.030
	2012	2010, 2011	0.869	0.017	0.048	0.045

870



871 **Figure Captions**

872 **Fig. 1** Temporal variations in the standard deviation of soil surface heights  $S_D$  and correlation  
873 length  $L_C$  estimated from measurements during seven days in 2012 performed at the M-III  
874 vineyard field. The annual mean values are  $\langle S_D \rangle = 2.2$  cm,  $\langle L_C \rangle = 6.2$  cm.

875 **Fig. 2.** Time-series of measured ELBARA-II  $T_B$  over the M-III vineyard during three years  
876 (2010-2012) at H ('o') and V ('x') polarizations and at the observation angle  $\theta = 40^\circ$ . The  $T_B$   
877 data are acquired ~ every 30 minutes but only data measured at 6 am are shown. Diurnal  
878 precipitation  $P$  is represented with vertical lines

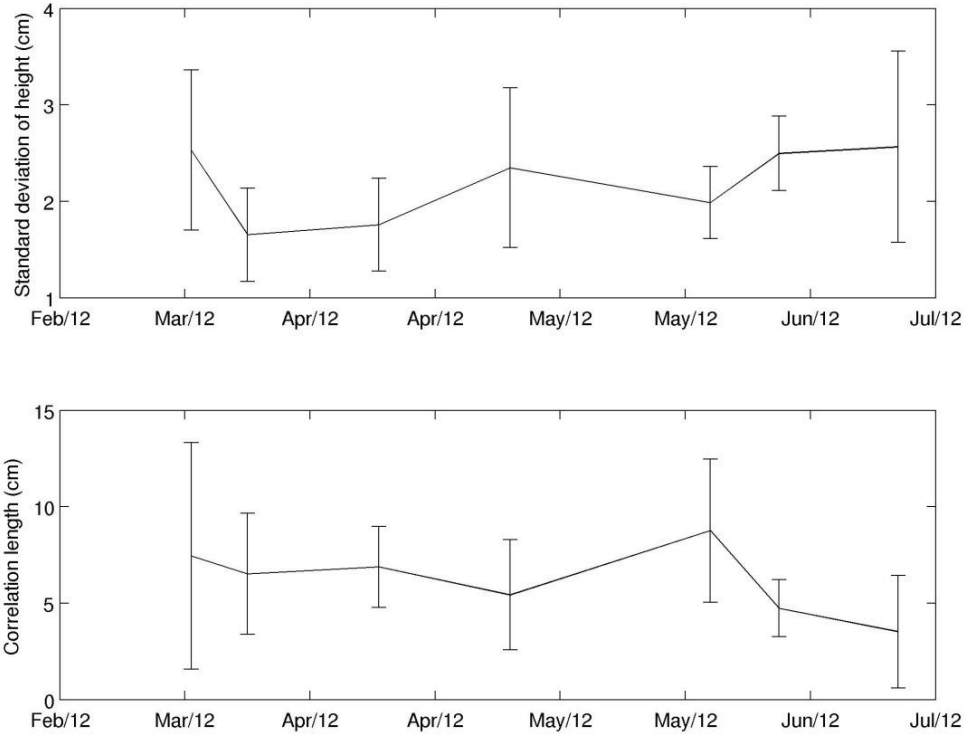
879 **Fig. 3.** Soil moisture  $SM$  (a) and optical depth  $\tau_{NAD}$  (b) retrieved with the multiangular 2-P L-  
880 MEB method applied to the measurements at the M-III site. The diurnal retrievals are shown  
881 for 6 am and 6 pm, respectively. These retrieved values are considered as a reference in this  
882 study. Diurnal precipitation is represented with vertical lines. In Fig 3b, the time-series of  
883 NDVI index obtained over the 250 m MODIS pixel including the M-III vineyard is shown.

884 **Fig. 4.** Scatter plot of retrieved values of the optical depth  $\tau_{NAD}$ , retrieved with the  
885 multiangular 2-P L-MEB method, versus the NDVI index obtained over the 250m MODIS  
886 pixel including the M-III vineyard. Retrieved values of  $\tau_{NAD}$  computed at 6 am and 6 pm are  
887 used.

888 **Fig. 5.** Scatter plots of the retrieved  $SM$  values versus the reference  $SM$  values for all  
889 methods: SCA-H (a), SCA-V (b), DCA (c), LPRM (d), 'Saleh' bi-angular (e), 'Saleh' bi-  
890 polarization (f) and 'Mattar' (g). Retrieved values of  $SM$  are computed at 6 am and 6 pm. In  
891 Fig. 5a-b-e-f-g, retrieved values of  $SM$  for years 2011 and 2012 are shown (the year 2010 was  
892 used for calibration). In Fig. 5c-d (for DCA and LPRM) retrieved values of  $SM$  for years  
893 2011, 2012 and 2013 are shown (no calibration was required).

894

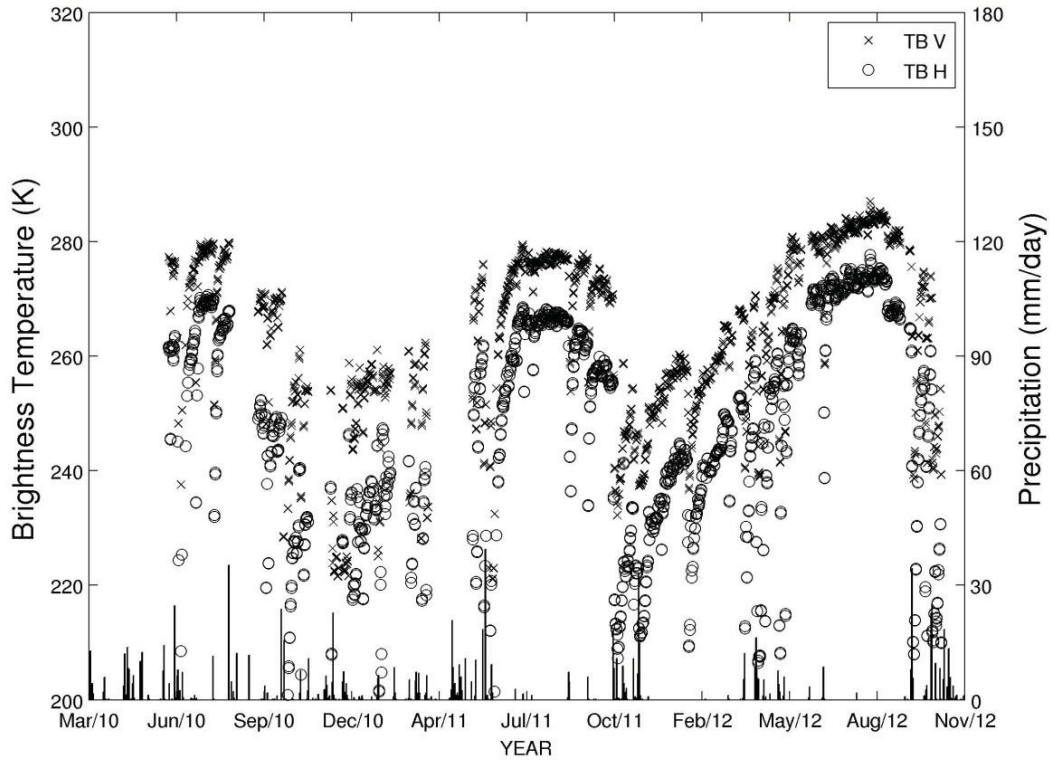
895 **Fig. 1** Temporal variations in the standard deviation of soil surface heights  $S_D$  and correlation  
896 length  $L_C$  estimated from measurements during seven days in 2012 performed at the M-III  
897 vineyard field. The annual mean values are  $\langle S_D \rangle = 2.2$  cm,  $\langle L_C \rangle = 6.2$  cm.



898

899

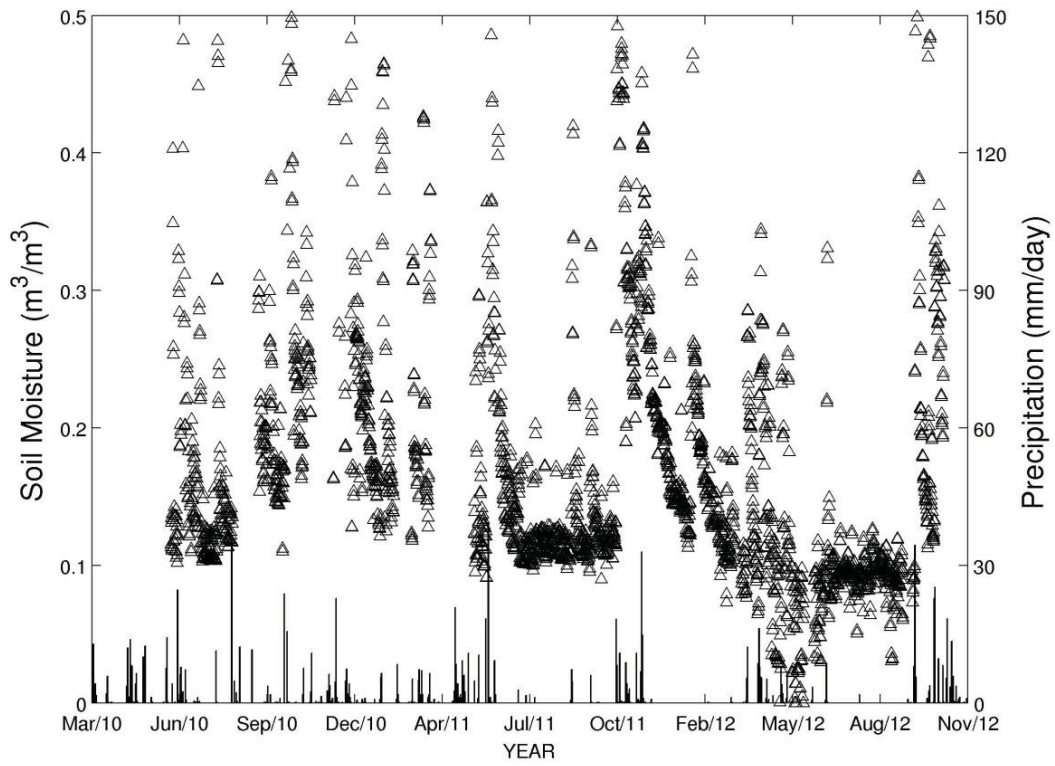
900 **Fig. 2.** Time-series of measured ELBARA-II  $T_B$  over the M-III vineyard during three years  
901 (2010-2012) at H ('o') and V ('x') polarizations and at the observation angle  $\theta = 40^\circ$ . The  $T_B$   
902 data are acquired  $\sim$  every 30 minutes but only data measured at 6 am are shown. Diurnal  
903 precipitation P is represented with vertical lines.



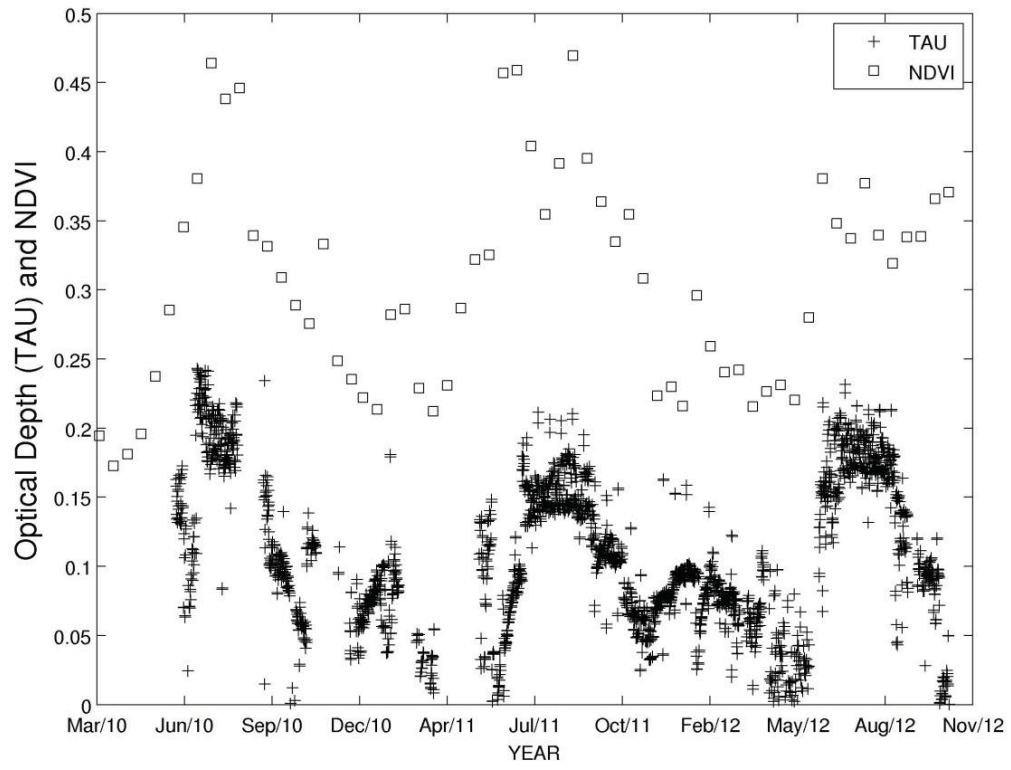
904

905 **Fig. 3.** Soil moisture SM (a) and optical depth  $\tau_{\text{NAD}}$  (b) retrieved with the multiangular 2-P L-  
906 MEB method applied to the measurements at the M-III site. The diurnal retrievals are shown  
907 for 6 am and 6 pm, respectively. These retrieved values are considered as a reference in this  
908 study. Diurnal precipitation is represented with vertical lines. In Fig 3b, the time-series of  
909 NDVI index obtained over the 250 m MODIS pixel including the M-III vineyard is shown.

910 a)



911



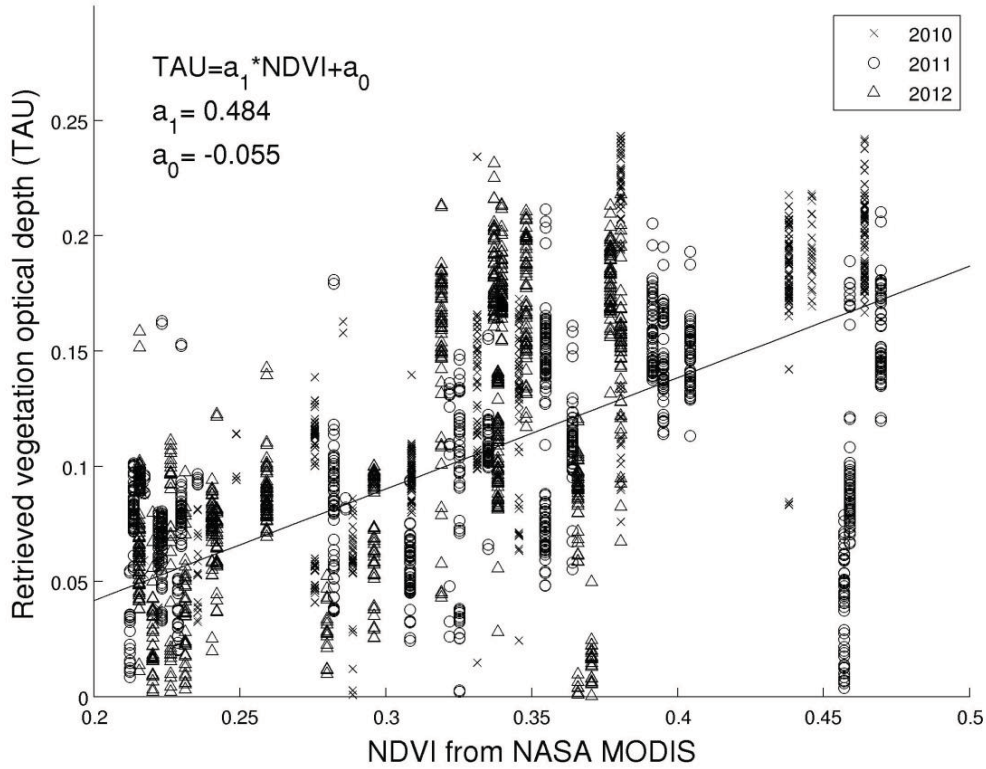
912

913 **b)**

914

915

916 **Fig. 4.** Scatter plot of retrieved values of the optical depth  $\tau_{NAD}$ , retrieved with the  
 917 multiangular 2-P L-MEB method, versus the NDVI index obtained over the 250m MODIS  
 918 pixel including the M-III vineyard. Retrieved values of  $\tau_{NAD}$  computed at 6 am and 6 pm are  
 919 used.

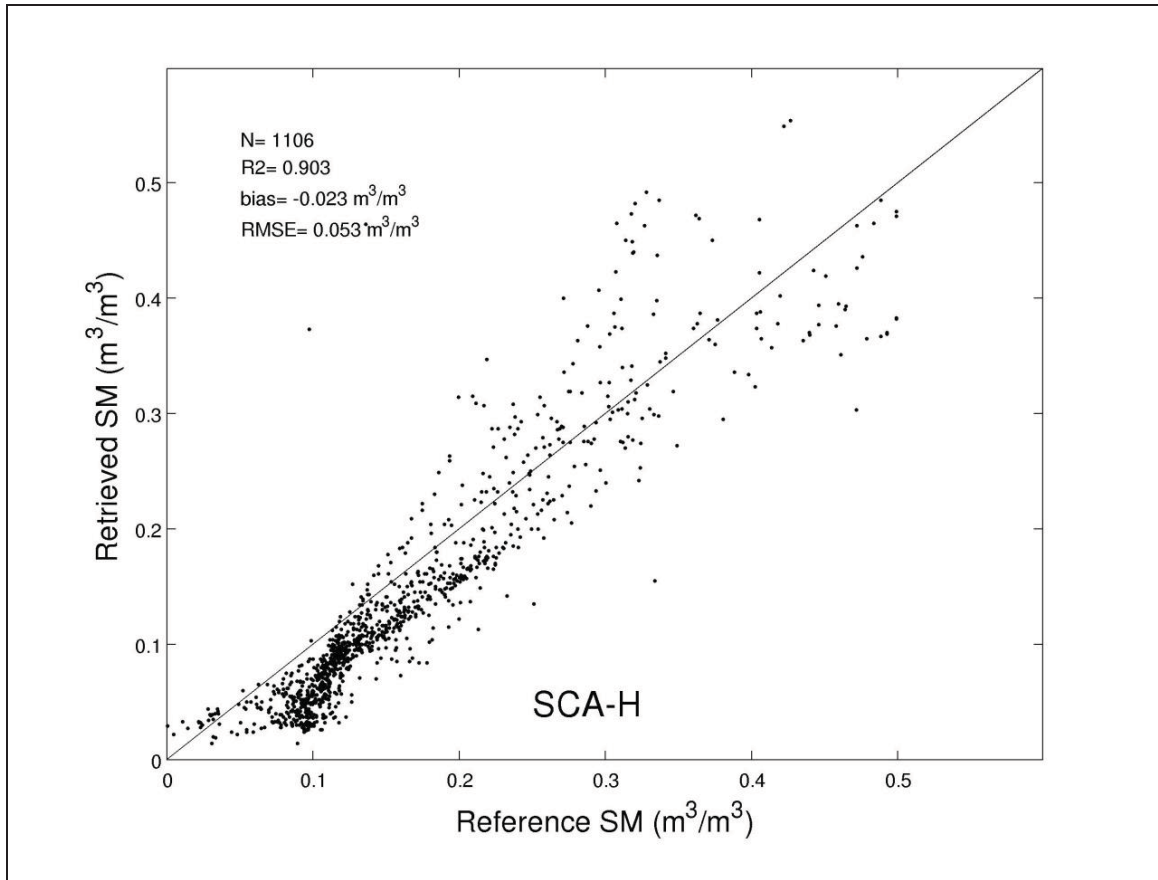


920

921 **Fig. 5.** Scatter plots of the retrieved SM values versus the reference SM values for all  
922 methods: SCA-H (a), SCA-V (b), DCA (c), LPRM (d), ‘Saleh’ bi-angular (e), ‘Saleh’ bi-  
923 polarization (f) and ‘Mattar’ (g). Retrieved values of SM are computed at 6 am and 6 pm. In  
924 Fig. 5a-b-e-f-g, retrieved values of SM for years 2011 and 2012 are shown (the year 2010 was  
925 used for calibration). In Fig. 5c-d (for DCA and LPRM) retrieved values of SM for years  
926 2011, 2012 and 2013 are shown (no calibration was required).

927

928 a)

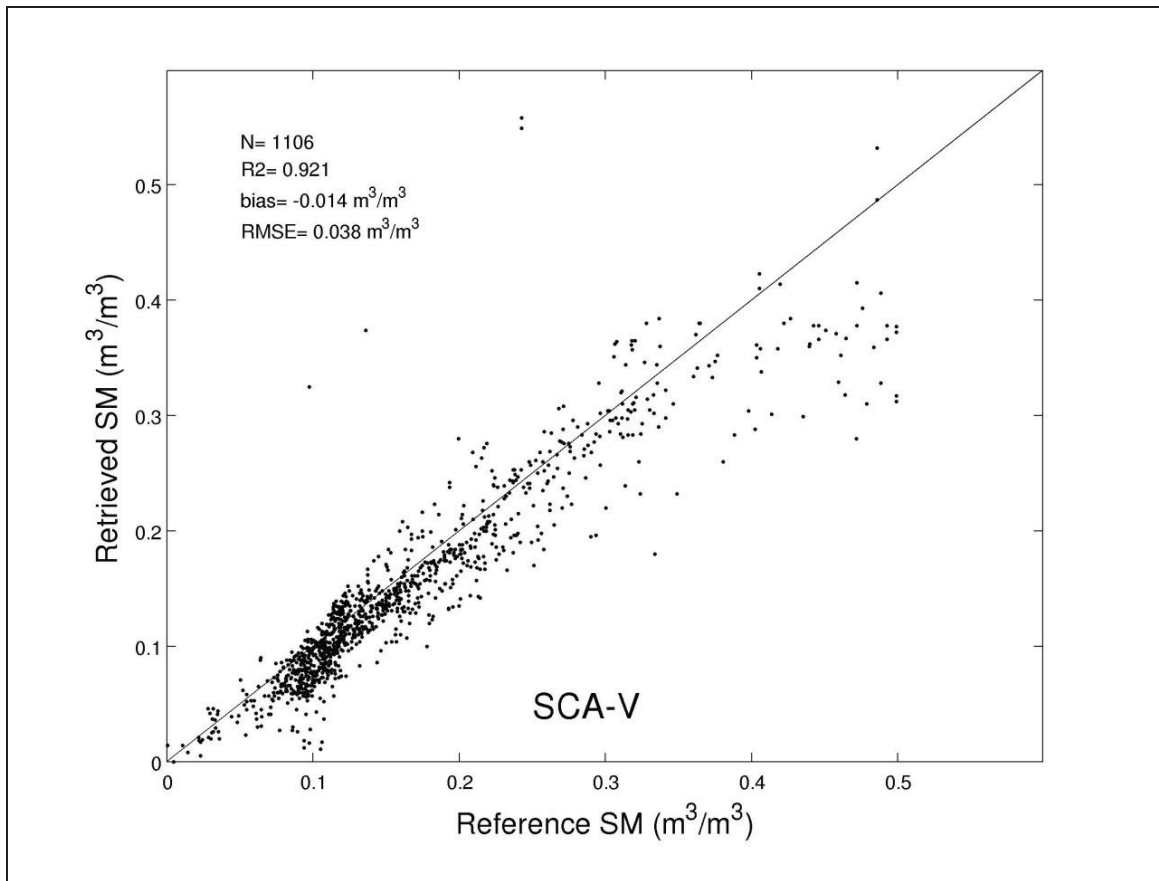


929

930



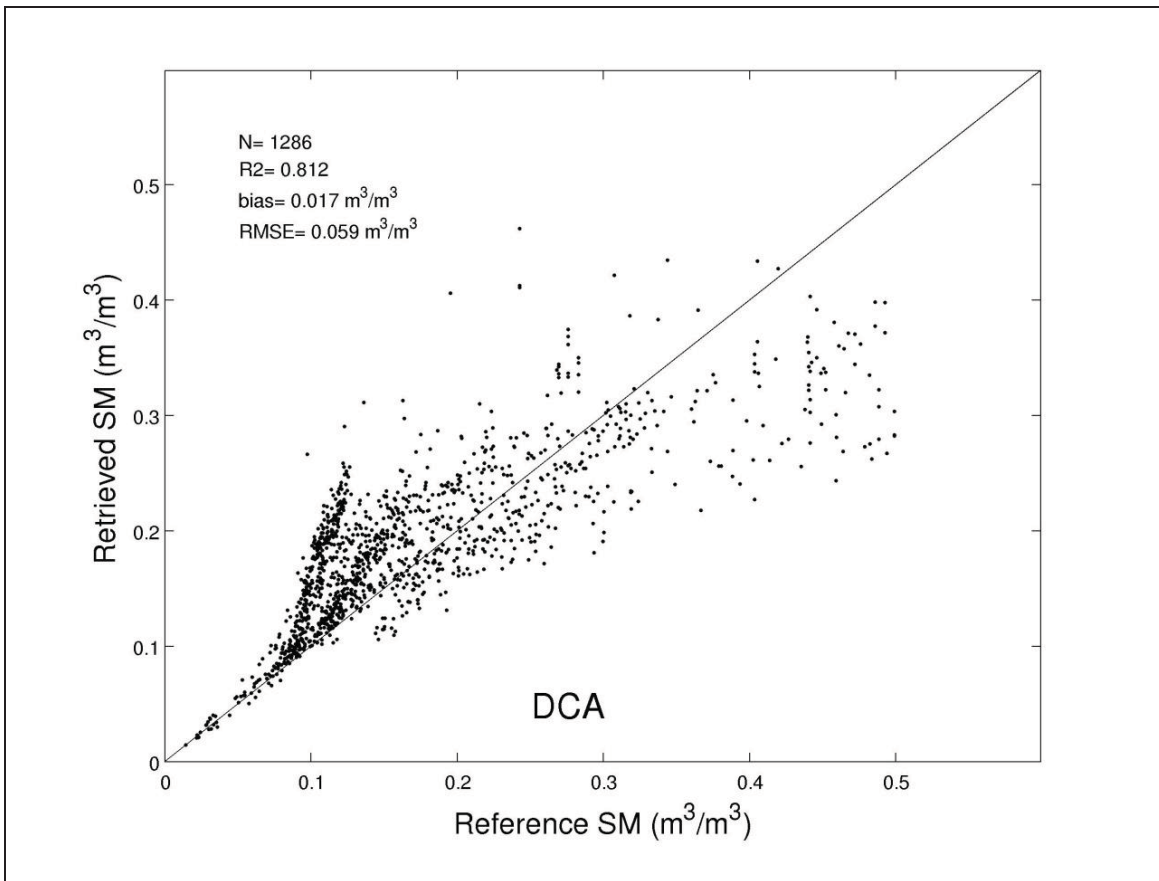
931 b)



932

933

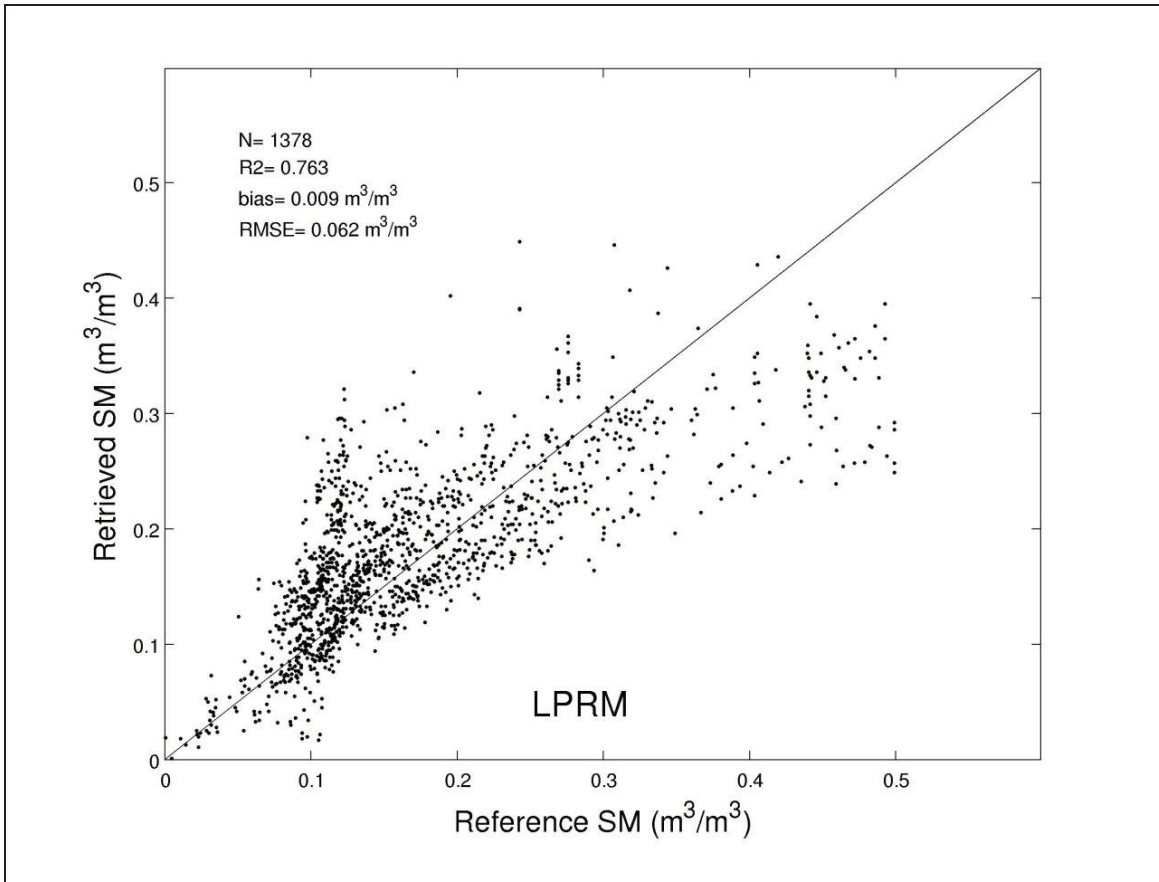
934 c)



935

936

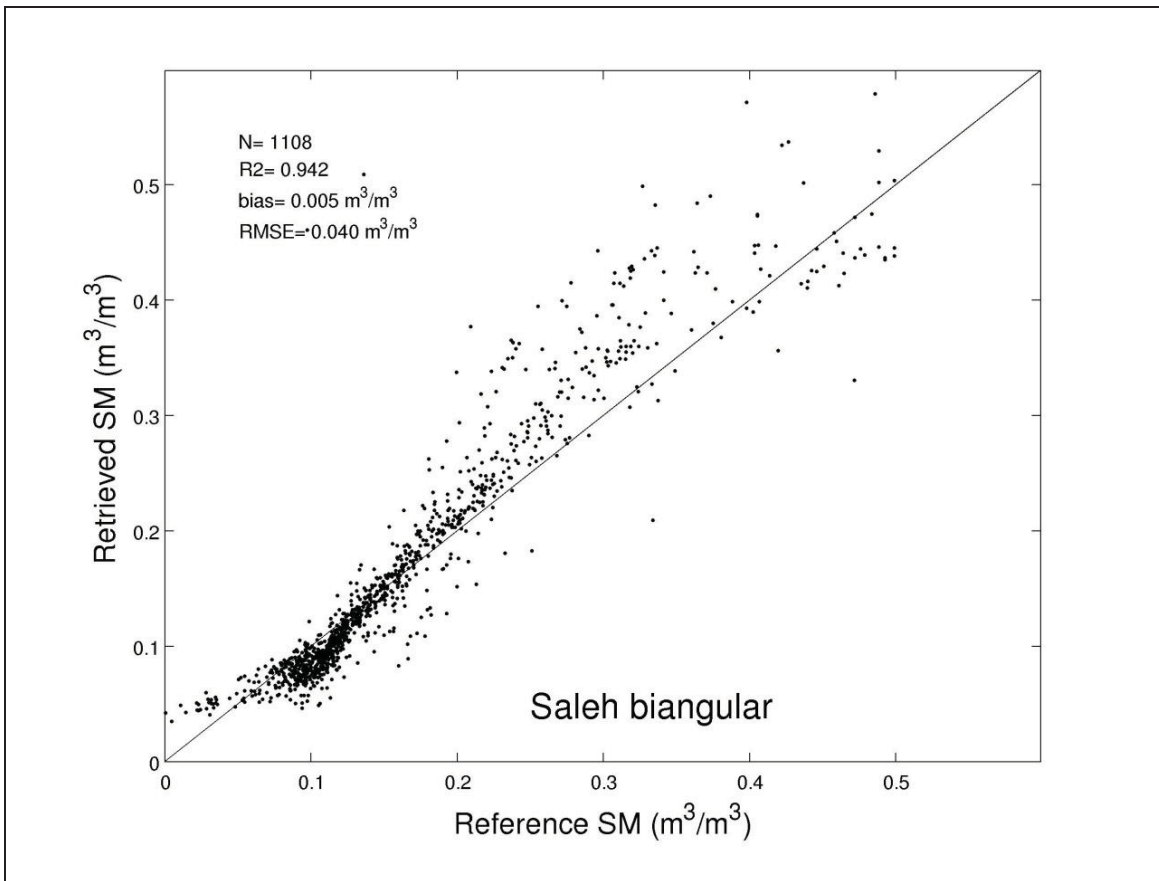
937 d)



938

939

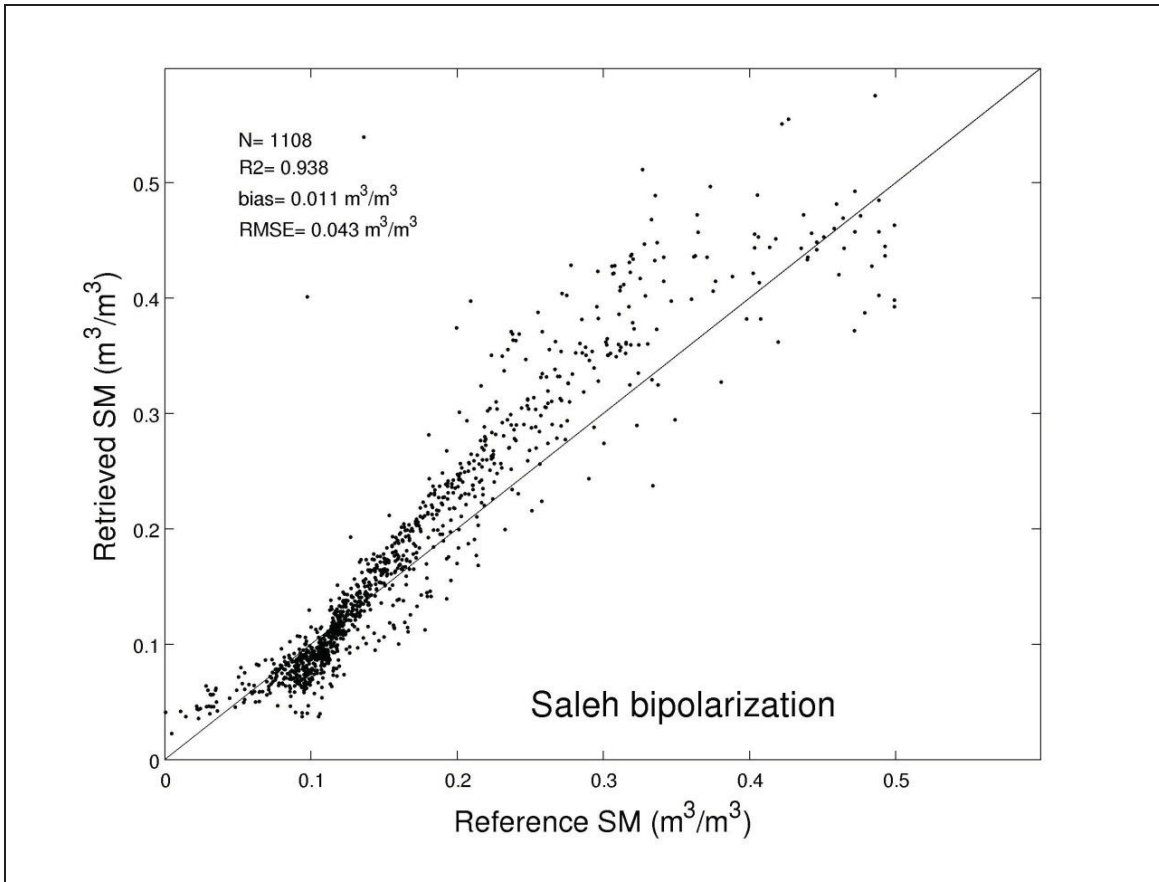
940 e)



941

942

943 f)

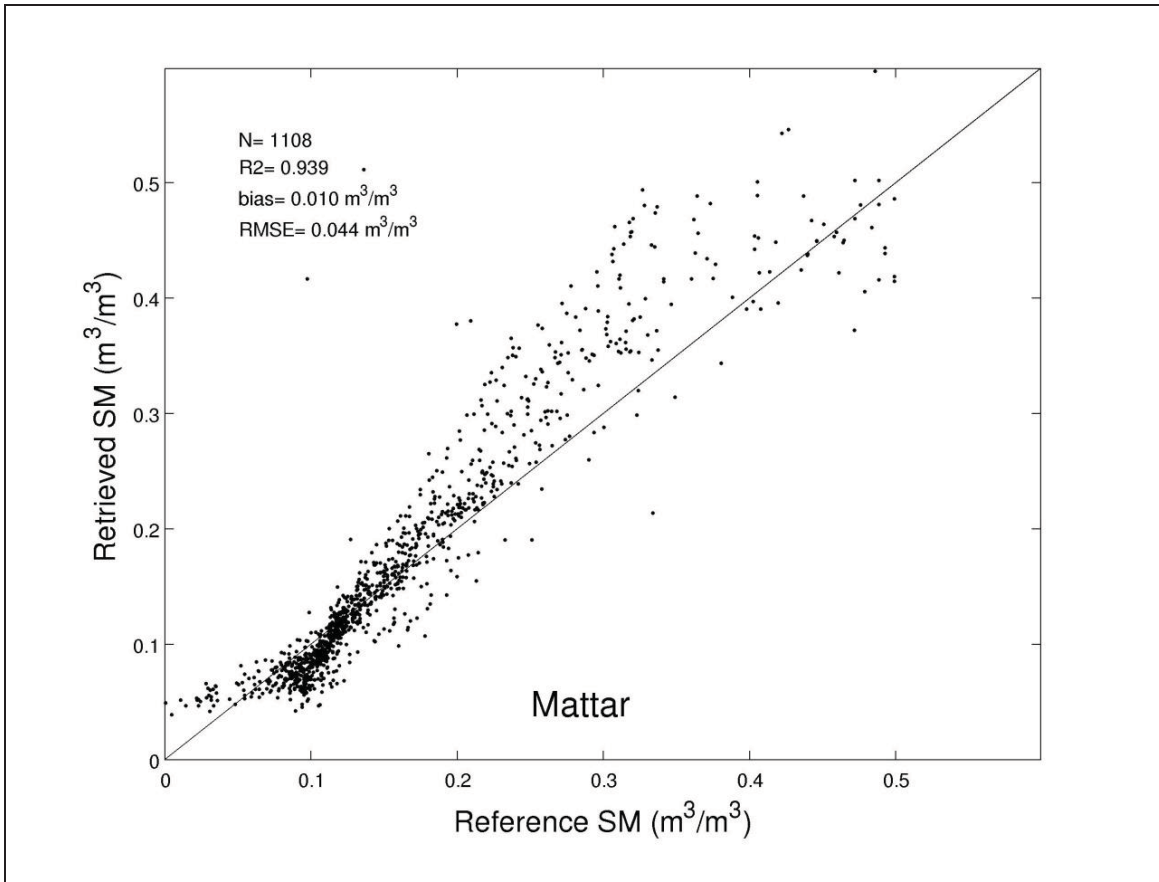


944

945

946

947 g)



948

949

950